UNDERSTANDING THE IMMUNE RESPONSE IN TUBERCULOSIS USING DIFFERENT MATHEMATICAL MODELS AND BIOLOGICAL SCALES[*]

DAVID GAMMACK[†], SUMAN GANGULI[†], SIMEONE MARINO[†],
JOSE SEGOVIA-JUAREZ[†], AND DENISE E. KIRSCHNER[†]

Abstract. The use of different mathematical tools to study biological processes is necessary to capture effects occurring at different scales. Here we study as an example the immune response to infection with the bacteria *Mycobacterium tuberculosis*, the causative agent of tuberculosis (TB). Immune responses are both global (lymph nodes, blood, and spleen) as well as local (site of infection) in nature. Interestingly, the immune response in TB at the site of infection results in the formation of spherical structures comprised of cells, bacteria, and effector molecules known as granulomas. In this work, we use four different mathematical tools to explore both the global immune response as well as the more local one (granuloma formation) and compare and contrast results obtained using these methods. Applying a range of approaches from continuous deterministic models to discrete stochastic ones allows us to make predictions and suggest hypotheses about the underlying biology that might otherwise go unnoticed. The tools developed and applied here are also applicable in other settings such as tumor modeling.

Key words. differential equations model, agent-based model, metapopulation model, compartmental model, partial differential equations model, granuloma formation, tuberculosis

AMS subject classifications. 68U20, 92B05

DOI. 10.1137/040603127

1. Introduction. Tuberculosis (TB) has been a leading cause of death in the world for centuries. Today it remains the number one cause of death by infectious disease worldwide—3.1 million deaths per year [77]. TB is not only one of our oldest microbial enemies, but it also remains one of the most formidable. An estimated one-third of the world population has been infected but does not show signs of TB disease (termed latent infection). Thus, there is a great need to elucidate the mechanisms of TB disease progression. Key issues are to understand the immune mechanisms involved in containing bacteria leading to control (latency). Interestingly, whether complete clearance of bacteria occurs is not known. Some data imply that upon exposure there is only a 30% chance of developing infection [10]. Whether the other 70% of individuals whom were inoculated either cleared infection or infection never took hold (or both) is not well understood. To this end, elaborating the primary immune response against *M. tuberculosis* (Mtb) is essential to understanding functional aspects leading to latency.

Primary infection usually develops in the alveoli of the lung after inhaling droplets containing Mtb. These are then ingested by resident scavenger cells called macrophages and begin to multiply [6] (this initiates the local response). These macrophages are poor at destroying Mtb, despite the fact that they readily eliminate other bacteria [47, 50]. Macrophages may burst due to the large number of bacteria multiplying

---

within them [78]. Infected macrophages and other scavenger cells, termed dendritic cells, circulate out of the lung to the draining lymph nodes where the specific immune response is initiated (which begins the global response) [34]. Here, the main immune controlling cells, known as $CD4^+$ T cells, are stimulated to become effector cells. These and other effector cells must then be recruited and migrate back to the site of infection where they interact with other cells at the site to form a functional granuloma.

Granuloma formation refers to the development of a roughly spherical structure comprised of cells, bacteria, and effector molecules in response to TB infection. The goal of a granuloma response is thought to be to "wall-off" bacteria and prevent spread in cases where bacteria cannot be cleared. Close proximity of cells to each other in this tightly packed structure may also facilitate cell-cell communication to enhance the host response. It is known that small, solid granulomas contain bacterial growth and spread while large, necrotic ones are not successful at containing bacteria and also result in severe tissue damage in the lung [59]. It is likely that whether an individual controls initial infection resulting in latency, or fails to control it and suffers active pulmonary TB, depends directly on granuloma formation and hence its function.

It is important to note that the local dynamics occurring within the lung regarding one granuloma and its formation may differ from the total lung response and finally from a more systemic response involving lymph nodes and other organs. Thus, considering the biological scale at which dynamics are acting is of key importance. For example, whether the success of one granuloma at controlling bacteria can be extrapolated to the entire lung and then to the body remains to be determined. Our hope is that this work will help begin to address this question.

Both the global and the localized immune responses are dependent on a number of factors including chemokines (chemotactic molecules secreted by immune cells), cytokines (pro- and antiinflammatory molecules secreted by immune cells), and immune effector cells. There exists a large body of experimental literature regarding these individual elements in the immune response in TB infection; however, little is known about the interaction among these elements that leads to distinct infection outcomes, namely latency or active disease. Our goal is to build computational models to elaborate the immune process with the ultimate goal of uncovering the role of the granuloma in achieving latency. There are multiple processes and different spatial and biological scales occurring during these dynamics, and our goal is to examine them using different mathematical methods.

To study the process of granuloma formation, we have developed several mathematical models based on different methods. We have applied these approaches over a range of biological scales. The processes described above can be studied at a single-cell scale [8, 62] to a scale of populations of cells [21, 45, 76]. Further, some of our studies focus on host-bacterial interactions at the local site of infection (cf. [76] and [22]) versus a more global system-wide involvement [46]. In each case, the mathematical tools required are different; thus, examining these processes over multiple scales can provide insights unattainable from any single approach.

Our goal in this work is to perform cross-comparisons between multiple mathematical models over different biological scales that we have developed to study the immune response to TB. Identifying features that are consistent over the various models may suggest key controlling factors that can be further studied experimentally. Identifying when the behavior of the discrete models results in the predicted mean behavior of the more deterministic ones (and when does it not) is an important

mathematical question that may have larger implications. Further, identifying features that are unique to particular models may suggest that elements operating at different scales are also important. Results obtained from this work can inform a larger set of both biological and mathematical systems.

2. Different models, different scales. To understand the immune response to infection with Mtb, we have developed a series of mathematical models, each using a different mathematical approach. Each of the models will be described below, but here we briefly outline the different approaches.

The first model used a system of nonlinear ODEs to describe the temporal dynamics occurring at the site of infection (the lung) [76]. Because our model was developed to model human infection, and no information is available describing infection dynamics in human lung tissue, we used as our reference space bronchoalveolar lavage (BAL) fluid. This is obtained via a process of washing the lungs with fluid that is then retrieved and cells and cytokines are measured. This gives a measure of the overall lung environment and thus is a more global indicator of infection status. These data are available from limited human studies and animal models, and it allowed us to compare our model results to data. Lessons learned from this detailed ODE model were applied in each of the other settings described below.

We then developed a model describing a more global picture of the immune response not limited to dynamics within the lung. Although bacteria initially enter into the lung and infection/disease manifests there, immune priming and activation occurs in the closest lymph node to the lungs, known as the draining lymph node. Trafficking between these physiological compartments is likely relevant, and so we expanded the ODE lung model into a two-compartment ODE model, tracking cell migration between the site of infection and the lymph node [45, 46].

Because our ultimate goal was to simulate granuloma formation, our next goal was to begin to capture spatial aspects of the immune response at the more local site of infection within the lung. To take advantage of the models we had already developed while making a first attempt at capturing spatial characteristics of the response, we applied a technique known as metapopulation modeling [22], which is a coarse-grid discrete spatial formulation of the system. This is the first step in moving the model from representing a virtual human model of TB infection based solely on temporal lung fluid measurements to representing spatial formation of a granuloma in human lung tissue. The original differential equation model [76] provided insight into key elements of the immune system responsible for containment of initial TB infection. That model assumes approximately a homogeneous distribution of cells and cytokines within lung fluid. To model granuloma formation, greater biological realism allowing for more detailed spatial heterogeneity was introduced into the model by accounting for movement of each of the cell populations within a discrete spatialization. Note that up until this point, direct inclusion of chemotactic signals, namely chemokines, was not included. A metapopulation approach works by creating a lattice that represents an area of lung tissue and then discretizing it into $n \times n$ grids. Within each grid we allowed a simplified version of the ODE model described above [76] to operate; then we defined new terms to account for migration or diffusion across the grids and at the boundaries. This increases the number of ODE systems by a factor of $(n \times n) - 1$. The details are described further below and have been submitted [22].

In another approach, we developed a PDE model [21]. Here our goal was to model only the innate response of macrophages before any adaptive immune response developed. This allowed us to predict if the system was progressing to active disease

or resolution (based on the boundary of the developing granuloma). To this end, we borrowed concepts from physics describing internal states for each of our macrophages, defined by their number of intracellular bacteria. We also now track forces acting on cells in the granuloma and monitor an internal velocity that made allowances for cells moving into or out of the site. Because we had no adaptive immune response present (i.e., no T cells or their effectors) this system could never achieve latency. This is expected as the stalemate achieved after infection with Mtb can only occur when an adaptive immune response is present.

Finally, rather than examining populations of cells at work in the infection site, we focused on the cells as individual agents by developing an agent-based model [62]. At this spatial scale, we could track the role of individual cells in the model and predict effects of actions on the forming granuloma. In this setting we were also able to track tissue damage (necrosis) as well as the more stochastic elements occurring within the lung during infection. This model is likely the most realistic in terms of the biology it describes, yet the rules established that govern its elements (cells, cytokines, bacteria, etc.) are basic.

An overriding approach that was applied in all of the model systems is the use of detailed uncertainty and sensitivity analyses. Uncertainty analysis allows for testing how variations in parameter space can affect outcome variable(s) of interest in the system. To this end an N-dimensional hypercube is created based on both ranges and distributions for all N parameters in the given model. This method is known as Latin hypercube sampling (LHS) [48]. The widest, biologically relevant range possible is used for all parameters. When applied correctly, this method identifies all relevant and distinct stable numerical solutions for the range of parameters given. Once variations in outcome variable(s) are identified, a partial rank correlation (PRC) is performed to identify which of the N parameters are most correlated with outcome values. Each PRC value generates a P-value that determines the significance; thus, even small correlations may be significant. This method was first applied in the context of differential equation models in [5]. We are the first to apply it in the context of agent-based modeling [62].

2.1. Model abstractions and assumptions. For each of the cell types we included, there are a series of assumptions we made based on known biological data that are consistent across all of the models. Additional assumptions are listed within each of the model subsections as relevant. The mathematical expressions are preserved between models whenever possible. Collective cell dynamics for all of the models are represented schematically in Figure 2.1. Effector molecules and their activities are not shown but are discussed for each model individually. Each of the models are a subset of this largest possible model. We provide a generalized mathematical description for this model in section 3.1.1. In section 3 we describe the specific differences.

1. *Macrophages*: In all of our models the most consistent element is that of macrophages. All the models account for resting and infected macrophages. All of the models also have activated macrophages, except the PDE model, as it focuses only on innate immunity, and this PDE model does not have T cells that are required to activate macrophages. The rules governing macrophage dynamics within each class are consistent from model to model: resting macrophages have a natural turnover at the infection site [71]; they become either infected (take up bacteria) or activated (via either cytokine effectors or T cells) [16, 52, 68]; infected macrophages either burst due to intracellular bacteria load or are killed by T cells [67, 78]. One feature of the agent-based model that we are not able to capture with any other model is a specific
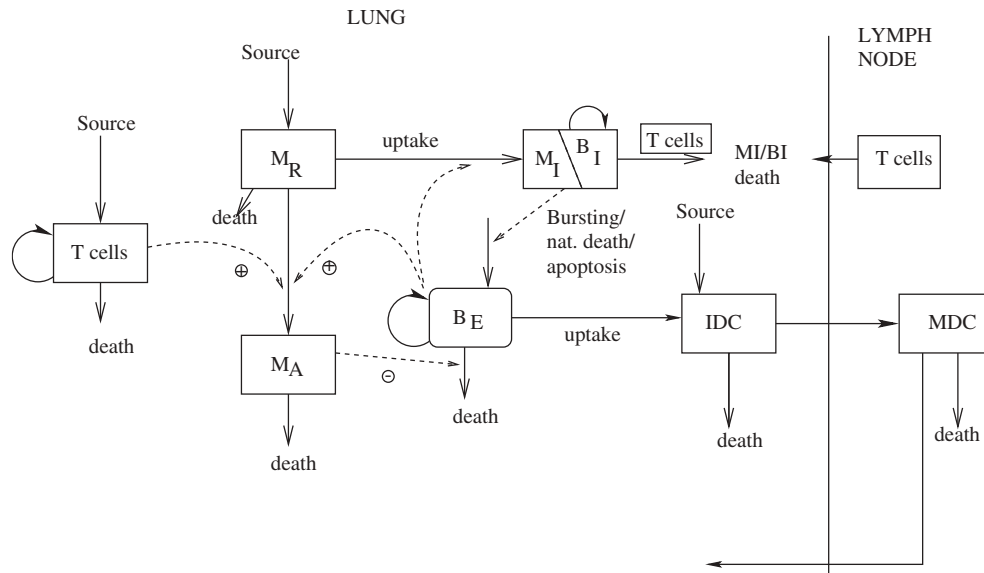
FIG. 2.1. *Cellular dynamics for global lung immunity to Mtb.* Effector molecules and their activities are not shown but are discussed for each model individually. M_R are resting macrophages, M_I are infected macrophages, M_A are activated macrophages, B_E are extracellular bacteria, B_I are intracellular bacteria, MDC are mature dendritic cells, and IDC are immature dendritic cells. All models are a subset of this larger model.

class of macrophages that have taken up bacteria but are not classified as either activated or chronically infected. There exists a short window of time during which they may either be activated or converted to chronically infected status. Because we track individual cells and their states in the agent based model we are able to capture this transitional class.

2. *T cells*: All of the models include a class of effector T cells, except for the PDE model that lacks adaptive immunity. The two global-scale ODE models distinguish between different subclasses of T cells (Th_0, Th_1, and Th_2 cells), while all the granuloma models consider one aggregate class. In fact, results from the ODE models indicate that information gained from distinguishing these subclasses is minimal, and so we collapsed them into one class for the more mathematically complex models. All T cells have a natural turnover and play two important roles: activation of resting macrophages and killing of infected macrophages. They also produce effector molecules.

3. *Effectors*: There are two classes of effector molecules that participate in adaptive immunity: cytokines (proteins that either up- or down-regulate cells to perform their functions) and chemokines (cytokines that have chemotactic properties). How we represent effectors is a key distinction between the different models. In the ODE models, we track specific cytokines and their known properties (IFN-γ, IL-10, IL-4, and IL-12) relevant to TB infection [17]. One feature adopted by the more complex models of granuloma formation was to simplify the model (and number of equations) by using the cells that secrete the cytokines as a surrogate for the effector molecules they produce. This is reasonable since there likely exists a proportionality between the two.

Since we do not track cell movement on a local level in the ODE models, chemo-

kines are not considered, and we have only a generic recruitment term. In contrast, all of the granuloma models track a value for chemokine that recruits cells to the infection site. Chemokine represents an aggregate of chemokines known to be involved in TB immunity and secreted by subclasses of macrophages and have a natural half-life (based on known chemokine values) [17].

4. *Bacteria*: In all of the models bacteria are tracked as both intracellular and extracellular [67]. In the ODE-based models these subsets are tracked as collective populations of cells, where as in the PDE and agent-based models we are able to track individual numbers within cells. In the PDE model, because it captures only innate immunity, we count the number of bacteria within each macrophage and classify the macrophages based on their internal state (load) of bacteria.

Bacteria grow logistically with respect to their environment and are either phagocytosed by macrophages or remain extracellular [66]. This is in fact a unique feature of the mathematical models: in a given tissue sample in the experimental setting it is not possible to track which bacteria are trapped within macrophages and which are present in tissue. Once intracellular they have two fates: they can either be killed along with their host macrophage when it is killed, or they can be released upon death of the host macrophage (becoming extracellular).

5. *Environment*: In the first ODE model, we track total immune dynamics in the lung, whereas in the two-compartmental model we track the dynamics occurring both within the lung and the closest lymph node as well as the trafficking between these compartments. Thus, these two models examine global immune dynamics during TB infection. In the last three models where we model granuloma formation, we consider only a small section of lung tissue as the environment and model dynamics occurring on the more local scale.

6. *General outcomes from all models*: We expect to see three general outcomes in all the models: *clearance*, where both extracellular and intracellular bacterial loads are zero; *latency* for global models or *containment* for granuloma models where bacterial load is stable and mostly intracellular; and *disease* for global models or *dissemination* for granuloma models, where bacterial load continues to grow and is dominated by extracellular bacteria, which is not in a steady state. Recall the PDE model does not exhibit containment, as this state is achieved only via adaptive immunity. To follow in section 3, we present details for each of the five modeling approaches that we used. We present the models, their baseline results, and dynamic model information. We highlight differences between each model as well as focus on key spatial factors affecting infection outcomes. The details for most of the models are omitted for brevity; instead we refer readers to the original papers. In section 4 we compare and contrast results for each of the models on both biological and mathematical scales, and in section 5 we conclude.

3. Model descriptions.

3.1. First approach: ODEs. To better understand the temporal dynamics of TB infection and immunity, we developed a virtual human model that qualitatively and quantitatively characterizes the cellular and cytokine control network operational in the total lung during TB infection [76]. Using this model we identified key regulatory elements in the host response.

3.1.1. The baseline ODE model. We modeled human TB infection in the lung using nonlinear ODEs. We developed a mathematical system based on the interactions of a number of key cells and cytokines known to be important in TB infection. Based

on their known and hypothesized interactions, we tracked both extracellular (B_E) and intracellular (B_I) bacteria and the following cell populations: lymphocytes (T_0, T_1, and T_2 cells), macrophages (resting-M_R, activated-M_A, and infected-M_I), and four cytokines (IFN-γ, IL-12, IL-10, and IL-4). Note that for this first modeling attempt we did not include every cell potentially involved (i.e., CD8+ T cells, cytotoxic T cells, NK cells, eosinophils, etc.) or every relevant cytokine (i.e., IL-2, TGF-β, TNF-α, etc.).

Generalized equations for the baseline model shown in Figure 2.1 are given below. A complete biological description for the baseline model can be found in [76]. To facilitate comparisons, we use the same parameter symbols and values of [76] and the following simplifying notation (for readability we have suppressed the (t) notation in all equations):

$$(3.1) \qquad f(x,a) \quad = \left(\frac{x}{x+a}\right),$$

$$(3.2) \qquad g(x,y,a,b) \quad = \left(\frac{x}{x+ay+b}\right),$$

$$(3.3) \qquad h(x,a,m) \quad = \left(\frac{x^m}{x^m+a^m}\right).$$

Macrophage equations.

$$(3.4) \qquad \begin{aligned} \frac{d}{dt}M_R &= s_{M_R} + \alpha_4(M_A+wM_I) + f(s_3,I_\gamma)f(c_8,B_T)\mu_{da}M_R \\ &+ f(B_T,c_{28})\alpha_{21}M_R + f(I_{10},s_8)k_4M_A \\ &- f(B_E,c_9)k_2M_R - f(I_\gamma,s_3)f(B_T,c_8)k_3M_R \\ &- \mu_R M_R, \end{aligned}$$

$$(3.5) \qquad \begin{aligned} \frac{d}{dt}M_A &= f(I_\gamma,s_3)f(B_T,c_8)k_3M_R - f(I_{10},s_8)k_4M_A \\ &- f(s_3,I_\gamma)f(c_8,B_T)\mu_{da}M_R - \mu_A M_A, \end{aligned}$$

$$(3.6) \qquad \begin{aligned} \frac{d}{dt}M_I &= f(B_E,c_9)k_2M_R + h(B_I,NM_I,2)k_{17}M_I \\ &- f\left(\frac{T_T}{M_I},c_4\right)(1-f(B_I,NM_I)p)k_{14}M_I - \mu_I M_I. \end{aligned}$$

Cytokine equations.

$$(3.7) \qquad \begin{aligned} \frac{d}{dt}I_\gamma &= s_g f(I_{12},s_7)f(B_T,c_{10}) + f(M_A,c_{14})\alpha_5 T_1 \\ &+ g(I_{12},I_{10},f_4,s_4)\alpha_7 T_0 - \mu_{I_\gamma}I_\gamma, \end{aligned}$$

$$(3.8) \qquad \frac{d}{dt}I_{12} = \alpha_8 M_a + \alpha_{22}M_I + g(I_\gamma,I_{10},f_5,s_5)\alpha_{10}M_R - \mu_{I_{12}}I_{12},$$

$$(3.9) \qquad \begin{aligned} \frac{d}{dt}I_{10} &= \left(f(B_T,c_{12})\alpha_{13}M_R + \alpha_{14}M_A\right)g(s_6,I_\gamma,I_{10}) \\ &+ \alpha_{16}T_1 + \alpha_{17}T_2 + \alpha_{18}f(I_{12},s_9)T_0 - \mu_{I10}I_{10}, \end{aligned}$$

$$(3.10) \qquad \frac{d}{dt}I_4 = \alpha_{11}T_0 + \alpha_{12}T_2 - \mu_{I4}I_4.$$

Lymphocyte equations.

$$(3.11) \quad \frac{d}{dt}T_0 = \alpha_1 \left(M_A + w M_I \right) + f \left(M_A, c_{15} \right) \alpha_2 T_0 - g \left(I_\gamma, I_4, f_1, s_1 \right) k_6 I_{12} T_0$$
$$- g \left(I_4, I_\gamma, f_2, s_2 \right) k_7 T_0 - \mu_{T0} T_0,$$

$$(3.12) \quad \frac{d}{dt}T_1 = \alpha_3 \left(M_A + w M_I \right) + g \left(I_\gamma, I_4, f_1, s_1 \right) I_{12} k_6 T_0 - \mu_{T1} T_1,$$

$$(3.13) \quad \frac{d}{dt}T_2 = \alpha_3 \left(M_A + w M_I \right) + g \left(I_4, I_\gamma, f_2, s_2 \right) k_7 T_0 - \mu_{T2} T_2.$$

Bacteria equations.

$$(3.14) \quad \frac{d}{dt}B_E = \alpha_{20} B_E - k_{15} M_A B_E - k_{18} M_R B_E$$
$$+ \mu_I B_I + h \left(B_I, N M_I, 2 \right) k_{17} N M_I - k_2 \left(\tfrac{N}{2} \right) f \left(B_E, c_9 \right) M_R,$$

$$(3.15) \quad \frac{d}{dt}B_I = \alpha_{19} B_I \left(1 - h \left(B_I, N M_I, 2 \right) \right) - h \left(B_I, N M_I, 2 \right) k_{17} N M_I$$
$$+ f \left(B_E, c_9 \right) k_2 \left(\tfrac{N}{2} \right) M_R - \mu_I B_I$$
$$- f \left(\tfrac{T_T}{M_I}, c_4 \right) \left(1 - p f \left(B_I, N M_I \right) \right) k_{14} N M_I.$$

Our first goal was to develop a model that represents the basic processes of the immune response to TB, including key players that had been identified in the literature. This original model has since been extended to include more mechanistic terms that had originally been included only phenomenologically [69]. A diagram indicating the interactions is given in Figure 2.1 if one considers only the lung compartment and no dendritic cells (which are relevant when we consider trafficking).

3.1.2. Parameter estimates. Once mathematical expressions were developed representing the interactions between the 8 cell populations and 4 cytokines, it was necessary to determine the values of the rate constants governing each of the interactions. Values for most rate parameters were estimated from published experimental data, with weight given to results obtained from humans or human cells and Mtb-specific data over results based on other bacterial species. Estimates obtained from multiple studies are represented as a range of values. For parameters that have a range and those for which no experimental data are available, we performed uncertainty and sensitivity analyses to obtain order-of-magnitude estimates as described above. We refer the reader to [76] for full details of our parameter estimation methods. Finally, we simulated the model by solving the differential equations using an appropriate numerical method. Our lab utilizes both packaged software (such as Mathematica and MATLAB) as well as a stiff solver algorithm based on Rosenbroch and Story that we coded in C/C++ to directly compare results of these different platforms for accuracy.

3.1.3. Results. The resulting model is a temporal simulation of infection after inoculum with Mtb in humans. The negative control, with no Mtb present in the system yields a result with resting macrophages at equilibrium (3×10^5/ml of lung fluid) and all other populations and cytokines at zero. The model also indicates that it is possible to be exposed to an initial bacterial inoculum and then clear infection with no memory of that response (i.e., skin-test negative). This outcome is plausible, as it

is thought that only 30% of individuals exposed to Mtb become infected (i.e., skin-test positive) [10]. The other outcomes for this more global dynamic model should be latency, primary disease, and reactivation. (Note the model can simulate reactivation, but, for brevity, we omit this discussion. See [76] for details.)

Figure 3.1 presents representative simulations of the virtual model for two given sets of parameter values, one leading to latency (Figure 3.1 A panels) and the other leading to active disease (Figure 3.1 B panels). Results are shown here only for bacterial and macrophage populations.
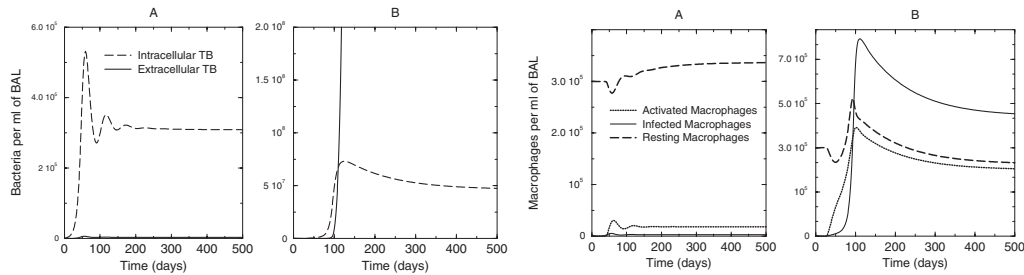

FIG. 3.1. *Model simulation results for the baseline ODE model. Results of bacteria load (left panel) and macrophage populations (right panel) per ml of lung fluid (BAL). Two simulations are shown for each, one leading to latency (A panels) and the other leading to active disease (B panels). The parameters that govern these different outcomes are shown in Table 3.1. All parameter values used are given in [76]. Differences between panels A and B are obtained by varying the parameter governing T cell killing of infected macrophages.*

Parameter values that govern the rates and behavior of interactions in the model may change from individual to individual and over time within an individual. Our analyses revealed that only a small number (only 6) of the 99 model parameters lead to different infection outcomes when varied—either latency or active disease (see [76]). A summary of these parameters is given in Table 3.1. Note that in this model, the role of macrophages (and their activation by INF-γ) and the importance of T cells both take on key roles in determining infection outcome. Finally, note that no spatial aspects are relevant here; even the included cellular recruitment terms do not govern infection outcome. This is in stark contrast to the remainder of the models discussed.

TABLE 3.1

Parameters that yield disease from latency in the ODE model. M_R are resting macrophages, M_I are infected macrophages, M_A are activated macrophages, and B_E are extracellular bacteria. Note that disease occurs if parameter value is either increased or decreased from baseline latency value.

Description	Disease occurs when value is	Latency value	Units
Chronic macrophage infection rate	increased	.9	/day
M_R activation rate	decreased	.04	/day
Maximal T cell killing of M_I	decreased	1.65	/day
Max. killing of B_E by M_A	decreased	$5x10^{-7}$	/M_A/day
Rate of INF-γ prod. by CD8$^+$ T cells	decreased	.4	pg/ml/day
IL-4 production by Th0 cells	increased	.03	pg/cell/day

3.2. Second approach: Multiple compartment ODE model. To capture global dynamics of Mtb infection and immunity, we developed a two-compartmental mathematical model that qualitatively and quantitatively examines important processes of cellular priming and activation [45]. These processes occur between the site

of infection (lung) and the nearest draining lymph node. The key cells mediating this process are the dendritic cells. During infection, macrophages are the prime target cells for Mtb, while after their activation they both kill intracellular bacteria and participate in a protective T cell mediated (Th$_1$) response. Dendritic cells play a major role in establishing an effective immune response. Immature or resting dendritic cells are present in high numbers at sites of infection (such as the lung) [28, 31, 32, 63, 72] at the onset of the inflammatory response; they are specialized for antigen uptake and processing [3, 4, 26]. After bacterial uptake, immature dendritic cells differentiate into the mature phenotype (mature dendritic cell): they reduce their phagocytic capability and begin expressing molecules for immune presentation and adhesion molecules for migration. The maturation-migration process of dendritic cells is enhanced during Mtb infection, while in contrast infected macrophages show little phenotypic change [12, 17, 23, 29].

As maturation occurs, dendritic cells migrate through lymphatic vessels and enter the T cell area of the draining lymph node, where they are performers of two main functions: facilitators of naive T cell recruitment and participants in antigen presentation. Once presentation occurs, naive T cells experience stages of differentiation, from naive to effector T cell. The first step from naive to precursor T cells takes place in the draining lymph node [42]. This phenotypic and functional change allows primed T cells to proliferate and then migrate through the efferent lymphatic vessels into the blood, eventually to the site of infection [73].

Thus, our two-compartment model extends the previous model (from section 3.1) by including relevant migration patterns between the draining lymph node and the lung as well as important processes performed by dendritic cells of antigen presentation and cellular activation. To this end, we added one physiological compartment (the lymph node) and five new variables (and consequently five equations) to the previous temporal model: one in the lung (immature dendritic cell-I_{DC}) and four in the draining lymph node compartment (mature dendritic cell-M_{DC}, naive T cells-T, Th$_0$ cells-T_0^{LN}, and the cytokine IL-12-I_{12}^{LN}). Lung model equations were slightly modified in order to account for these new variables (see [45]) for the equations). Below we show only the equations that have been added to the baseline model described in section 3.1.1, and we retain the abbreviated notation for f, g, and h. See Figure 2.1 for the complete model.

IL-12 equation.

$$(3.16) \qquad \frac{d}{dt}I_{12}^{LN} = \delta_1 M_{DC} - \mu_{I_{12}^{LN}} I_{12}^{LN}.$$

Naive T-cell equation.

$$(3.17) \qquad \frac{d}{dt}T = s_T + \delta_2 M_{DC} - \lambda T - \mu_T T - \delta_4 M_{DC} T.$$

Th$_0$ equation.

$$(3.18) \qquad \frac{d}{dt}T_0^{LN} = \delta_4 M_{DC} T - \delta_5 T_0^{LN}\left(1 - \frac{T_0^{LN}}{\rho}\right) - \xi T_0^{LN}.$$

Mature dendritic cell equation.

$$(3.19) \qquad \frac{d}{dt}M_{DC} = f(B_E, \delta_{11})\phi\delta_{10}I_{DC} - \mu_{M_{DC}} M_{DC}.$$

Immature dendritic cell equation.

$$(3.20) \qquad \frac{d}{dt} I_{DC} \quad = s_{I_{DC}} - f(B_E, \delta_{11}) \delta_{10} I_{DC} + f(B_E, \delta_9) \delta_8 I_{DC} - \mu_{I_{DC}} I_{DC}.$$

3.2.1. Parameter estimates. In order to scale lung and lymph node compartmental cell trafficking, we use volumetric measure units, namely cells per cm^3 of tissue (both in the lung and in the lymph node). We calibrate initial conditions of our virtual model to match estimates of cell distributions in the two compartments. To guide our study a nonhuman primate animal system of TB was studied concurrently for data comparison [7, 18]. This nonhuman primate system has provided data for parameter estimation as well as data for validation of our virtual model simulations (see [45] for details about parameter estimation and nonhuman primate data comparison). Experiments in the nonhuman primate model are now being performed to test some of our predictions.

3.2.2. Results. The results of the two-compartmental model are in line with the previous temporal lung model simulations (cf. section 3.1 and [76]). In fact, in our virtual latent infection scenario (see Figure 3.2), the majority of bacteria are intracellular, and levels of extracellular bacteria are below the level of detection of current assays. This confirms experimental results where no bacteria were found in the lung of latently infected mice and in nonhuman primates [7].
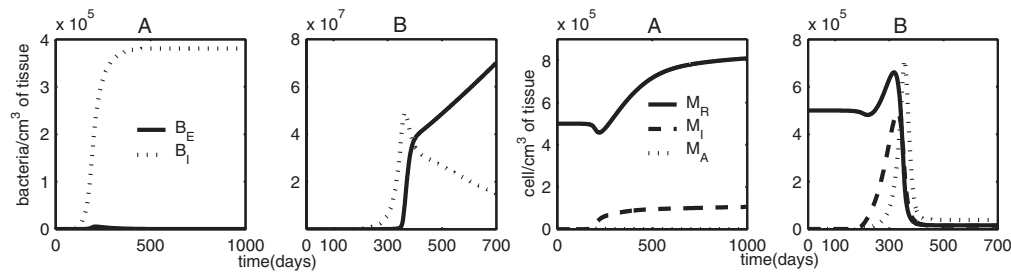

FIG. 3.2. *Model simulation results for the 2-compartment model. Results of bacteria load (left panel: log scale, extracellular-B_E, and intracellular-B_I) and macrophage populations (right panel: log scale, resting-M_R, infected-M_I, and activated-M_A) per cm^3 of tissue. Two simulations are shown for each, one leading to latency (A panels, 1000 days) and the other leading to active TB (B panels, 700 days). The parameters that govern these different outcomes are shown in Table 3.2. All parameter values used are given in [45]. Differences between panels A and B are obtained by varying a set of parameters; see [45].*

Our model also predicts that during latency lymphocyte populations at the site of infection are mainly of Th$_0$ type, with very low levels of effector T cells (Th$_1$ and Th$_2$, results not shown). In fact, during peak infection, comparing latency to primary TB, a faster migration of Th precursor cells from the draining lymph nodes to the lung may explain the host ability to contain bacteria in the latency outcome (see [45]).

Our two-compartmental model simulations highlight the role of phagocytic cells (macrophages and dendritic cells) in initiating and directing adaptive T cell immunity, in particular the key action of dendritic cells in establishing and maintaining latency. Dendritic cells have multiple roles: they participate in innate immunity by internalizing bacteria at the site of infection and represent the main link between innate and adaptive immunity via trafficking from the lung to the lymph node. This

model suggests how increasing the rate of bacterial uptake by resident immature dendritic cells could be advantageous both in terms of a stronger innate response and as a more efficient link to an effective adaptive response.

Results from our sensitivity analysis (summarized in Table 3.2) again indicate that the role of T cell killing of macrophages is still important (as shown in the previous model—see Table 3.1), but we are now able to keep track of other processes early stages, such as T cell differentiation, dendritic cell migration, and Th$_0$ trafficking.

TABLE 3.2

Parameters that yield disease from latency in the two compartment ODE model. Parameters above the line are nonspatial, while those below govern spatial dynamics. DC are dendritic cells, M_A are activated macrophages, and B_E are extracellular bacteria. Comparison with Table 3.1 reveals a number of new parameters are significant for this model.

Parameter description	Disease occurs when value is	Latency value	Units
Chronic macrophage infection rate	increased	0.4	/day
Growth rate, B_E	increased	5e-3	/day
M_A deactivation rate	increased	0.36	/day
IFN-γ extra source	decreased	700	(pg/ml)/day
IL-12 production rate by mature DC	decreased	3.5e-3	pg/(day*mature DC)
Mature DC deactivation rate	increased	0.02	/day
Max. Th1 differentiation (from Th0)	decreased	0.1	(ml/pg)/day
Max. Th2 differentiation (from Th0)	increased	0.05	/day
Mature DC-T cell interaction	decreased	1e-4	ml/(day*mature DC)
Max. rate of apoptosis/T cell action	decreased	0.5	/day
% of Th0 migrating out of the draining lymph node into the blood	decreased	0.9	/day
Immature DC baseline turnover	decreased	500	(immature DC/ml)/day
Max. Immature DC migration	decreased	0.2	/day

In fact, the main result of our two-compartmental model is that a delay in either dendritic cell migration to the draining lymph node or T cell trafficking to the site of infection can alter the outcome of Mtb infection or define a progression from latency to active TB or a possible reactivation scenario (see Table 3.2 and [45] for details). Delayed dendritic cell migration can be simulated by decreasing immature dendritic cell turnover rates or immature dendritic cell migration rates from the site of infection to the draining lymph node. T cell trafficking can be altered by decreasing the percentage of precursor T helper cells migrating out of the draining lymph node. We can also modulate the intensity and duration of antigen presentation in the draining lymph node by changing the mature dendritic cell-Naive T cell interaction term or mature dendritic cell half-life. These delays are due in part to specific spatial issues that will be addressed in more detail in the next sections (metapopulation, PDE, and agent-based models), with particular emphasis on the site of infection (the lung) where granuloma formations occurs locally.

Our results are in line with the idea that a fast dendritic cell turnover at the site of infection as well as strong activation by dendritic cells leading to maximal antigen presentation and production of key cytokines (inducing the most protective T cell response) could represent a viable strategy for the development of a new generation of treatments against Mtb [23, 33].

3.3. Third approach: Metapopulation model. One approach we pursued to extend the temporal model presented above to a spatio-temporal model is a metapopulation framework. In this section we describe our metapopulation model of the adaptive immune response to Mtb infection. Further details are presented in the appendix.

A metapopulation approach means that the spatial domain is partitioned into a number of distinct sites, each containing subpopulations. Dynamics of these subpopulations are locally coupled, reflecting migration of subpopulations between sites. The metapopulation approach has been applied widely as a method of incorporating spatial heterogeneity into population models. Most of this work has been done for ecological or epidemiological models, such as [24, 35, 36, 37, 38, 56, 57]. We applied the metapopulation framework at the cellular level, in order to study spatial aspects of the immune response to Mtb infection.

The spatial domain for this model, and for the subsequent spatio-temporal models described below (the PDE and agent-based models), is a two-dimensional cross-section of alveolar lung tissue. For the metapopulation approach this spatial domain is discretized into an $n \times n$ lattice of compartments. Each compartment contains subpopulations of various cell types. As described in section 2.1, we made the simplifying assumptions of removing all cytokine variables (instead representing their effects by the cells that secrete them) and collapsing the three T cell subpopulations of the temporal ODE model into a single T cell population. We introduced a new variable to represent chemokine concentrations. Thus, the model includes the following types of populations: extracellular bacteria (B_E), intracellular bacteria (B_I), resting macrophages (M_R), infected macrophages (M_I), activated macrophages (M_A), T cells (T), and a chemotactic effector molecule that we include for the first time, chemokine (C).

Hence the model consists of $7n^2$ variables: $B_{E\,(i,j)}$, $B_{I\,(i,j)}$, $M_{R\,(i,j)}$, $M_{I\,(i,j)}$, $M_{A\,(i,j)}$, $T_{(i,j)}$, and $C_{(i,j)}$ for $0 \le i,j < n$. Here (i,j) are the indices of the $n \times n$ lattice of compartments (see Figure 3.3). Nonlinear ODEs govern the dynamics of these subpopulations. The terms in these ODEs represent (1) local interactions between subpopulations within each compartment and (2) movement of subpopulations between compartments. The local within-compartment dynamics of this model are based on the dynamics of the temporal model described in section 3.1 and are portrayed in the lung compartment of Figure 2.1 (not including dendritic cells). The equations representing these dynamics are given in the appendix.
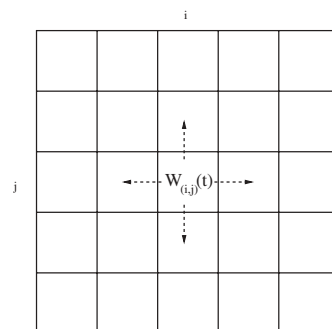

FIG. 3.3. *A depiction of the spatial environment of the metapopulation model, which consists of an $n \times n$ lattice of compartments. $W_{(i,j)}(t)$ represents the subpopulation of a generic variable type, W in compartment (i,j) at time t. If W is one of the cell types, and it is allowed to move, $W_{(i,j)}(t)$ migrates to the four adjacent compartments, as indicated.*

In addition to the local interactions, the ODEs for subpopulations in adjacent compartments are locally coupled via terms that represent movement of subpopulations. In this model, resting macrophages, activated macrophages, T cells, and chemokine are allowed to move. Hence, the ODEs for $M_{R\,(i,j)}(t)$, $M_{A\,(i,j)}(t)$, $T_{(i,j)}(t)$,

and $C_{(i,j)}(t)$ include movement terms. The key feature of the movement terms are a set of "movement coefficients" for cell type w in compartment (i,j): $\alpha_{i,j,S}^w$, $\alpha_{i,j,R}^w$, $\alpha_{i,j,L}^w$, $\alpha_{i,j,U}^w$, and $\alpha_{i,j,D}^w$.

These five movement coefficients represent, respectively, the proportion of cells that move right (R), left (L), up (U), and down (D) out of the compartment, and that remain stationary (S) within the compartment. To capture chemotaxis, these coefficients are calculated as a function of the chemokine gradients between the compartment and its neighbors. Further details are given in the appendix. The movement coefficients are recalculated at each step, as a function of the changing chemokine environment. Hence, the system of $7n^2$ ODEs in fact evolves over the course of the simulation.

3.3.1. Parameter estimates. For parameter estimates, we relied on the work of [76] in surveying the biological literature for estimates of the kinetic parameters (i.e., those related to local, within-compartment dynamics). The new parameters introduced in this model were related to chemokine production and diffusion, chemokine-driven recruitment of immune cells, and movement of immune cells. Estimates for chemokine production parameters were obtained from experimental data found in the literature. Recruitment and movement parameters were varied over a wide range to study their effects on infection outcome. To solve this metapopulation system, we used standard numerical solvers for ODEs coded into the C programming language. These solvers were modified so that the movement coefficients were also recalculated at each step as a function of $C_{(i,j)}(t)$, as described above.

We studied simulations using a metapopulation model with the spatial domain consisting of a 5×5 lattice of compartments. Initial conditions consisted of a background level of resting macrophages distributed across the lattice and an initial infection of 25 extracellular bacteria in the center compartment (i.e., compartment $(2,2)$). Note that since neither extracellular bacteria nor infected macrophage subpopulations were allowed to migrate between compartments in this model, infection was restricted to the center compartment. This allowed us to focus on the processes of recruitment and migration in the local neighborhood of a forming granuloma contained within the center compartment.

To determine the spatial dimensions, we chose to make each compartment (and in particular the center compartment) large enough to contain a single granuloma. There is evidence that poorly formed granulomas may have radii of 2 mm or larger [7, 13]. To ensure that the center compartment of the lattice was large enough to contain such a granuloma, we assumed that each compartment corresponded to 5 mm $\times$ 5 mm of alveolar lung tissue, making the dimensions of the entire lattice 25 mm $\times$ 25 mm.

3.3.2. Results. Across a wide range of parameter values, we observed two distinct classes of outcomes. We believe these outcomes can be characterized as corresponding to distinct *local* outcomes of infection: (1) containment and control of bacterial growth and (2) uncontrolled bacterial growth. These outcomes were distinguished according to extracellular bacterial levels within the center compartment. In that sense, our criteria and results are qualitatively similar to the results of the temporal ODE models, as presented in sections 3.1 and 3.2. However, results of the metapopulation model represent a *spatially local* immune response to a single focal point of infection, since the spatial domain of the model represents a small portion of lung tissue and an initial infection therein. Unlike the temporal ODE model, results of the metapopulation model are not interpreted as corresponding to global infection outcomes for the individual, such as active disease or latency.

Figure 3.4 shows results for bacterial and macrophage subpopulations in the center compartment from two simulations. Panels A show results from a simulation leading to control of bacterial growth. All subpopulations—including extracellular bacteria—achieve steady-state equilibria.[1] Panels B, on the other hand, show results corresponding to uncontrolled growth of extracellular bacteria, as can be seen clearly in the bacterial population plot.
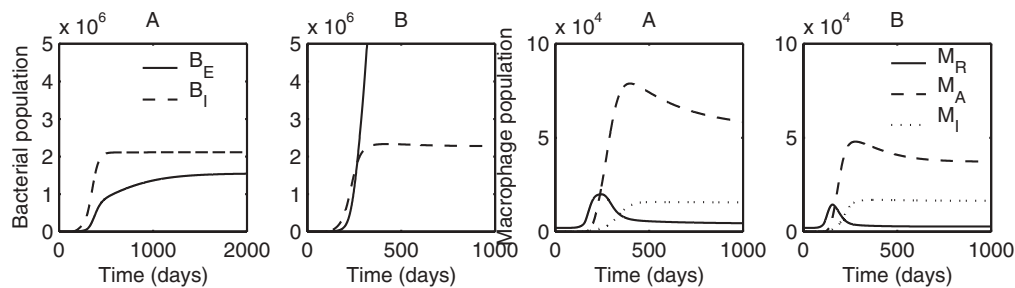

FIG. 3.4. *Simulations of the metapopulation model. Results corresponding to control of bacterial growth (A panels) and uncontrolled bacterial growth (B panels), respectively. Shown are bacterial (left panels: extracellular-B_E and intracellular-B_I) and macrophage (right panels: resting-M_R, infected-M_I, and activated-M_A) populations in the center compartment of a 5×5 lattice. All parameter values used are given in [22]. Differences between panels A and B are obtained by varying the parameter governing the rate of killing of bacteria (B_E) by activated macrophages.*

Beyond temporal dynamics like those shown Figure 3.4, the metapopulation model allowed us to examine spatial distributions of immune cells, as well as study the effects of various spatial parameters on infection outcome. One technique for visualizing this spatial result is surface plotting. The domain of such surface plots is the two-dimensional lattice of compartments. A surface plot for population W at time t is formed by plotting $W_{(i,j)}(t)$ as the height of the surface over compartment (i,j).

Figure 3.5 depicts the spatial distributions of various subpopulations (from top to bottom: extracellular bacteria (B_E), resting macrophages (M_R), infected macrophages (M_I), activated macrophages (M_A), T cells (T), and chemokine (C)) over the course of a simulation leading to uncontrolled bacterial growth. Each column shows the spatial distributions of these populations at a different time point. Uncontrolled growth of extracellular bacteria can be seen in the first row. The second and fifth rows show the development of steady-state spatial distributions of resting macrophages and T cells during uncontrolled bacterial growth. Resting macrophages and T cells are recruited into the boundary compartments by chemokine and then move chemotactically towards the center compartment, due to the spatial chemokine pattern shown in the bottom row of Figure 3.5. T cells maintain a maximum level at the center compartment, whereas resting macrophages initially concentrate in the center compartment (at time 150 days, for example), but this resting macrophage peak collapses as there is a turnover of resting macrophages to infected and activated macrophages in the center compartment (due to the presence of extracellular bacteria and T cells, respectively). This demonstrates continuous recruitment of immune cells during the process of granuloma formation, even though the immune response process is unsuccessful in controlling bacterial growth.

---

[1]Note that bacterial population in panel A is plotted over a longer time course than the other plots, in order to show that extracellular bacteria approach a steady state.
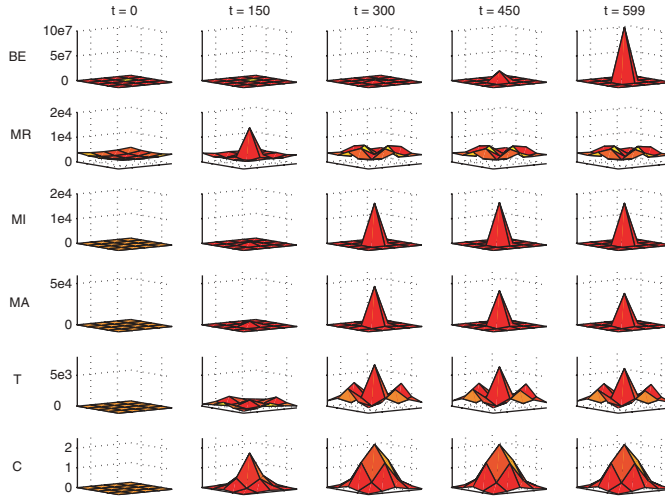
FIG. 3.5. *Surface plots of the spatial distribution of extracellular bacteria (B_E), resting macro-phages (M_R), infected macrophages (M_I), activated macrophages (M_A), T cells (T), and chemokine (C) variables at times $t = 0$, 150, 300, 450, and 599 days during a simulation leading to uncontrolled bacterial growth in the metapopulation model.*

Results in panels A of Figure 3.4 represent a baseline simulation in which bacterial growth is successfully controlled. We extensively explored the dynamics of all the parameters in the model with respect to this baseline simulation: using the set of parameter values that yielded the baseline simulation, we varied each parameter to determine whether biologically reasonable variations in the given parameter yielded a change from control of bacterial growth to uncontrolled bacterial growth. Table 3.3 summarizes these results. As can be seen from the table, the majority of new parameters led to such a stable-state change.

TABLE 3.3
Parameters that yield uncontrolled bacterial growth from latency in the metapopulation model. Parameters in the top half of the table are kinetic parameters, while the bottom half lists spatial recruitment and movement parameters. M_R are resting macrophages, M_I are infected macrophages, M_A are activated macrophages, B_E is extracellular bacteria, and C are chemokines.

Parameter description	Disease occurs when value is	Containment value	Units
Chronic macrophage infection rate	increased	0.5	/day
M_R activation rate	decreased	0.2	/day
M_A deactivation rate	increased	0.4	/day
Rate of killing of B_E by M_A	decreased	1.25×10^{-6}	/M_A/day
Death rate, T cells	increased	0.33	/day
Growth rate, B_E	increased	0.03	/day
Max. recruitment of M_R via C	decreased	10^3	M_R/day
Max. recruitment of T via C	decreased	10^4	T/day
rate of movement of M_A	decreased	0.2	/day
rate of movement of T cells	decreased	0.4	/day
rate of movement of C	decreased	1.0	/day

Recall that significant new features of the metapopulation model included the following spatial mechanisms: chemokine-driven recruitment of resting macrophages and T cells as well as chemotactic movement of resting macrophages, activated macro-

phages, and T cells. As listed in Table 3.3, we found that infection outcome is sensitive to each of the parameters governing recruitment and movement. This is strong evidence for considering spatial aspects of the immune response in determining infection outcome. We argued in [22] that many of these spatial aspects can be explained by the idea that modeling the spatial domain introduces a "delay" between initial infection of macrophages and secretion of chemokine in the center compartment, and subsequent recruitment and migration of immune cells. This may be compared with the results of [46] as described above in section 3.2, which also found that a delay in T cell trafficking to the site of infection can significantly influence infection outcome.

Interestingly, the metapopulation model revealed that spatial interactions *outside* the granuloma itself, i.e., outside of the center compartment, play a key role in infection outcome. This can be seen most strikingly in considering χ_A, the parameter for the rate of movement of activated macrophages. Decreasing χ_A from its baseline value led to uncontrolled bacterial growth. This result was counterintuitive, since it appeared that activated macrophages played a role only within the center compartment by eliminating extracellular bacteria. Therefore, increasing their rate of movement should, if anything, be detrimental to the immune response, by removing more activated macrophages from the site of extracellular bacterial growth.

These results led us to reexamine the role that activated macrophages play in the adaptive immune response. We identified two mechanisms to explain the result with respect to χ_A: activated macrophages contribute to T cell proliferation and chemokine production. Decreasing χ_A had the effect of decreasing the number of activated macrophages that migrate out of the center compartment. This reduces the strength of the chemokine signal that is produced in the periphery of the lattice, and it also reduces the amount of T cell proliferation in those locations. Together these have the combined effect of weakening the immune response sufficiently to result in uncontrolled infection. Thus, the model revealed that activated macrophage migration may be an essential aspect of the immune response. Activated macrophage migration *away* from the granuloma may serve as a way of signaling and strengthening the adaptive immune response at the periphery of the site of infection via mechanisms such as chemokine production and T cell proliferation. These results were unattainable using only a temporal modeling approach.

3.4. Fourth approach: PDE model. PDEs have been widely used to model the spatial movement and temporal development of densities of cells [9, 30, 39, 40, 49, 53, 54, 55, 64, 65]. For example, the models of Keller and Segel [39, 40] were developed to examine how cells move via directed cell movement (chemotaxis). Before discussing our model [21], we briefly discuss the mathematical techniques used to model processes in general biological systems that will be utilized here. In this section we discuss spatio-temporal modeling of Mtb infection using PDEs. Modeling temporal effects and processes of Mtb infection were discussed in section 3.1, and the first steps towards modeling more global spatial effects were developed using a compartmental model (see section 3.2). The metapopulation model of section 3.3 was developed as a discretized version of a PDE model. Essentially all movement terms were finite difference approximations to the continuous diffusion and chemotaxis terms we discuss here. However, in the metapopulation model it was assumed that bacteria were confined to a single compartment. Although this allowed us to study the effects of immune cell movement on infection progression, it does not help us estimate the size of the granuloma or the importance of bacterial movement parameters. Here we show how PDEs can be used to track the spatial progression of Mtb infection at a local scale.

In order to develop a spatial model of the innate immune response to Mtb infection, some of the biological processes we needed to include are granuloma size and growth, recruitment of resting macrophages to the site of infection, cell movement inside the granuloma, and phagocytosis. Mathematically, in its simplest form, a granuloma can be thought of as an amalgamation of cells that form a compact spheroid. This spheroid then expands, or contracts, depending on the current state of the immune cells and bacteria present. Therefore, a granuloma can be described as a multicellular spheroid in much the same way as a tumor. The main difference is that a tumor develops via the rapid proliferation of cells, whereas, for granuloma growth, bacteria infect macrophages and cells are recruited to it. While research on the spatial aspects of Mtb has been limited, modeling of tumor spheroids has progressed rapidly. Ward and King [74, 75] used reaction-diffusion equations to study the growth of avascular tumors. They assumed that the tumor spheroid is well packed (has no-voids) and that cell proliferation, death, and active movement contribute to a volume increase or decrease which causes the cells to move. This type of movement is often referred to as an internal (or bulk) velocity. Using this formulation, it is straightforward to calculate the tumor radius at any given time. In our model we use these ideas to model the growth of a granuloma. To capture recruitment of cells, we can choose boundary conditions such that cells may enter or leave the granuloma (we discuss this more fully below). Movement inside the granuloma is captured in two terms, a standard diffusion term and a chemotaxis term. These types of terms have been studied extensively by others; for example, see [9, 30, 39, 40, 49, 53, 54, 55, 64, 65]. Phagocytosis is the act of engulfing foreign objects by host immune cells. In our model we consider resting macrophages that engulf bacteria one at a time. Using an internal-states formulation we constructed a "ladder of infection" such that we have M_w, $w = 0, \ldots, N$, where the index, w, indicates the number of intracellular bacteria within that class of macrophage. Therefore, we track the density of macrophages infected with a specific number of bacteria, and hence the total density of intracellular bacteria. This is unique to the formulation of the PDE model. This formulation allows us to consider phagocytosis as a process whereby macrophages step up the infectivity ladder.

We now give an overview of our model of the innate immune response to Mtb (for a full account of this model see [21]). There are five dependent variable types in our model: extracellular bacteria, $B(t,x)$, macrophages (uninfected and infected), $M_w(t,x)$, $w = 0, \ldots, N$, a bacteria produced chemokine, $C(t,x)$, the internal velocity of cells within the granuloma, $v(t,x)$, and the granuloma radius, $R(t)$.

Figure 3.6 shows how the different cell types interact within this PDE model. The notation for the variables in this model differ slightly to other models presented here. This is because, rather than having different macrophage classes for resting/infected and chronically infected macrophages, we use a *ladder* of infection. Here, a macrophage is given by $M_w(t,x)$, $w = 0, \ldots, N$, where w is an integer which denotes the number of bacteria inside a particular macrophage.

3.4.1. Model. In the lung tissue, we assume that extracellular bacteria grow exponentially, in the absence of any immune cells. Unlike the metapopulation, we do not assume that within a compartment all cells are well mixed. In their paper, Sannomiya et al. [58] showed that bacteria release chemokines on contact with tissue. Therefore, we assume that extracellular bacteria release a chemokine that attracts resting macrophages to the growing granuloma. Macrophages are then able to phagocytose and kill bacteria. However, bacteria can proliferate within their host macrophage, and if
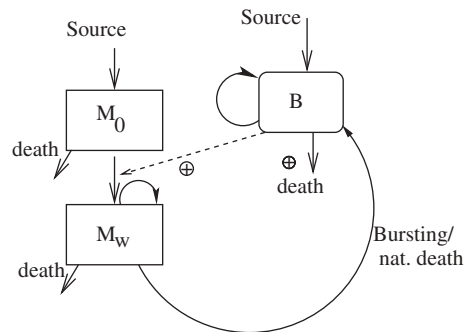
FIG. 3.6. *Cellular dynamics for PDE model. M_0 are uninfected macrophages, M_w are infected macrophages, with w the number of intracellular bacteria, and B are extracellular bacteria. Compare with Figure 2.1, which includes adaptive immunity and multiple compartments.*

the macrophage harbors too many bacteria it loses functionality [12]. In particular, we assume that a macrophage loses its ability to phagocytose extracellular bacteria and kill intracellular bacteria once the intracellular bacteria levels reach some critical threshold. Once bacteria levels within a macrophage have surpassed this threshold, the macrophage will eventually die: either via age or via bursting due to excessive numbers bacteria [70]. We assume that all cell types move via diffusion and that, once produced, chemokine diffuses through the tissue. In addition, resting macrophages also move via chemotaxis. Finally, all cells in the granuloma are affected by an internal velocity. This was first discussed by Ward and King [74]. Essentially, this velocity is generated via the volume reduction and growth due to bacterial growth, phagocytosis, death, and other movement into and out of the granuloma. The model presented here is one-dimensional, and, therefore, the size of the granuloma is measured by $R(t)$, the one-dimensional analogue of the granuloma radius.

3.4.2. Parameter estimates. A full list of parameter values can be found in Gammack, Doering, and Kirschner [21]. Parameters were mostly taken from [76] with the estimates for cellular movement and flux taken from various sources [53, 54, 74, 75]. To solve the equations, we first nondimensionalized and then used the no-voids condition to eliminate the extracellular bacteria equation to obtain an expression for internal velocity. The moving boundary of the granuloma is then mapped onto the unit interval via a scaling of the spatial variable: $x = R(t)\,\rho$. The equations are solved sequentially: first, $v(x,t)$ is found using the trapezium method; then $R(t)$ is updated; then the equations were approximated using the NAG routine D03PCF [51]. These steps are then repeated with $B(x,t)$ found at each time point by using the no-voids condition.

3.4.3. Results. Before discussing the results of the PDE model, we first recall that it differs from models presented in other sections in one fundamental way: it was developed to model the innate immune response. Therefore, as discussed in Gammack, Doering, and Kirschner [21], only two outcomes are possible: continued granuloma growth (granuloma radius, $R(t)$, grows unbounded) or control of infection (granuloma radius, $R(t)$, decays to zero). We would expect that, with the addition of other immune cell populations, this growth would either be stopped (leading to a solid granuloma) or continue, leading to a necrotic granuloma. Additionally, the PDE description of the innate immune response to TB is specific to a given region of the

lung and tracks the progression of a single granuloma. Therefore, unlike the temporal
models presented in sections 3.1 and 3.2, but similar to the metapopulation model is
section 3.3, all results are spatially local effects rather than global results pertaining
to an individual host.

TABLE 3.4
*Parameters that yield to uncontrolled bacterial growth (disease) from containment in the PDE
model. Spatial parameters are shown below the line, where kinetic parameters are above.*

Parameter description	Disease occurs when value is	Containment value	Units
Extracellular bacteria growth rate	increased	10^{-8}	/sec
Macrophage infection rate	decreased	10^{-5}	/sec
Rate of intracellular killing of bacteria	decreased	10^{-14}	/sec
Flux of chemokine across the granuloma boundary	increased	10^{-14}	m/sec
Flux of resting macrophages across the granuloma boundary	decreased	10^{-10}	m/sec
Rate of macrophage chemotaxis	decreased	10^{-3}	$\text{m}^2/\text{sec}/M$

The PDE model simulations show that phagocytosis, intracellular bacterial killing,
and bacterial growth (both extra- and intracellular) have an important effect on the
development of a granuloma (see Table 3.4). The specific effects of these parameters
are discussed fully in Gammack, Doering, and Kirschner [21]. In summary, decreasing
rates of phagocytosis and bacterial killing lead to granuloma growth (as bacteria are
allowed to survive and replicate), whereas increasing growth rates lead to increased
numbers of bacteria that cannot be dealt with by the innate immune response. In
Figure 3.7 two sets of graphs are shown. It can be seen that for control of infection,
both bacterial populations die out, and macrophage populations decay to zero. This
decay in macrophage population occurs since the granuloma is shrinking. When in-
fection progresses, extracellular bacteria become the abundant population. Figure 3.8
shows how the size (radius) of the granuloma changes over time for the two outcomes
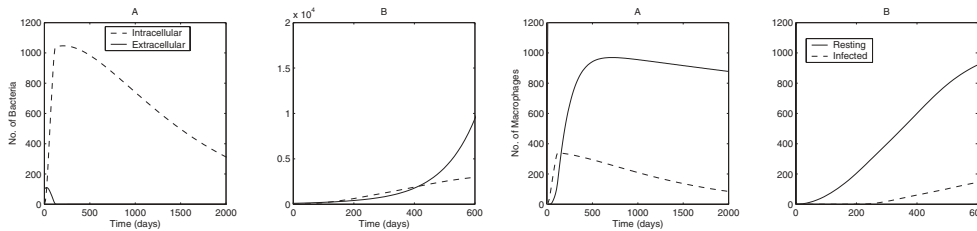discussed above.

FIG. 3.7. *Plots showing bacterial and macrophage levels over time in the PDE model. Panels A
show results where the granuloma is contained, while panels B show results where the granuloma
continues to grow. The chemotaxis parameter, χ, was set to zero in panels B.*

Additional results presented in Table 3.4 relate to the flux (Q_M, Q_C) and chemo-
taxis (χ) parameters. In this current work, we varied these parameters over a wide
range rather than the restricted range discussed in our previous paper. The param-
eter Q_M is, effectively, a source term for macrophages, and that it behaves like a
bifurcation parameter is intuitive. Thus, decreasing its value leads to a reduction in
macrophage numbers inside the granuloma, and hence allows the continued growth of
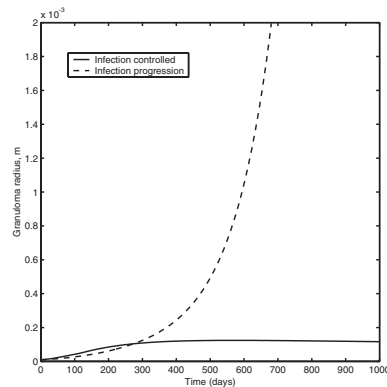bacteria. Chemokine flux, Q_C, acts in the opposite way. As flux increases, the amount

Fig. 3.8. Radius plots from the PDE model. *Two plots of the granuloma radius, $R(t)$, against time. Parameter values chosen to highlight granuloma growth and containment.*

of chemokine at the boundary decreases and macrophage recruitment falls. Therefore, if chemokine flux is too high, the amount of macrophages present in the granuloma will be too small to combat infection. Finally, we have found that decreasing the rate of macrophage chemotaxis, χ, also leads to disease. This likely follows since macrophages recruited into the granuloma are not moving directly toward bacteria, thus giving bacteria an additional advantage over the immune response.

3.5. Fifth approach: Agent-based model. The models described in the previous sections do not capture the spatio-temporal heterogeneity of individual cells (macrophages and T cells), in terms of states of cells and their spatial locations. Representing such cellular-level heterogeneity may be essential to properly capturing the process of granuloma formation. In order to improve our understanding of this complex system, we developed an agent-based model that includes representations of individual entities, their states, and their basic behavioral rules all residing in a two-dimensional abstraction of lung tissue [62]. The agent-based model allowed us to define more clearly individual interactions among entities at the cellular level and observe resulting dynamics at the tissue level.

In an agent-based modeling framework, elements of the system being modeled are represented primarily as *discrete* agents. This is in contrast with the differential equation frameworks used in the models described in the previous sections, in which elements are represented by continuous population variables. Moreover, these discrete agents typically reside within some spatial environment and interact with one another and with the environment *locally* (with respect to the environment).

Agent-based modeling is an extension and outgrowth of cellular automata models, which have been applied widely in theoretical biology [15]. Agent-based models have been applied to social sciences (e.g., [2, 14, 60, 61]) and more recently to biological sciences (e.g., [1, 25, 43, 44]).

The agent-based model we developed has the following components: the spatial toroid environment, which is a representation of a section of lung tissue; discrete agents representing macrophages and T cells; continuous variables representing extracellular bacteria and chemokines; rules describing behavior and interactions of agents and continuous entities; and the time-scales on which the rules are executed. The environment is made large enough to contain the relevant dynamics entirely within its interior. Chemokines create a field where macrophages and T cells move toward

higher concentrations. In this setting, larger size lattices (i.e., the torus) do not affect the dynamics of T cells, macrophages, or the infection outcome.

In contrast with previous models, the agent-based model distinguishes between chronically infected macrophages defined as those that cannot be activated and containing many intracellular bacteria versus infected macrophages defined as macrophages with a few resident bacteria that have a short window during which they can still be activated by T cells. The agents and rules that govern their behaviors as well as implementation features are described in detail in [62].

3.5.1. Parameter estimates. Many parameters were obtained from published data [19, 22, 76]; however, many could not be reliably estimated from experimental results (such as the probabilities involved in the stochastic rules). In order to explore the parameter space and determine which parameters are significant to infection outcome, we applied both uncertainty and sensitivity analyses. We performed uncertainty analysis by using the Latin hypercube sampling (LHS) [5, 27], which is an extension of the Latin square sampling. The LHS sample size was 1000. The sensitivity analysis was performed by evaluating partial rank correlation coefficients (PRCCs) for input parameters for each outcome variable. We study the behavior of the model over a range of parameter values described in more detail in [62]. To quantitatively analyze the effects of varying parameters, we used the total extracellular bacteria as the primary measure of infection outcome.

3.5.2. Description of dynamics. The initial conditions consist of a background level of resting macrophages distributed randomly on the lattice and a low initial infectious dose of extracellular bacteria placed in a small number of microcompartments near the center of the lattice. A given number (four) of "source compartments" are placed on the lattice where new cells can be recruited. Resting macrophages undergo random walks initially, in the absence of any chemokine on the lattice. Simulation begins when a resting macrophage comes in contact with bacteria, either killing bacteria or becoming infected. Due to chemokine secretion by these infected macrophages and chemokine diffusion, a chemokine gradient is created. This gradient attracts the remaining resting macrophages to surround infected macrophages. Moreover, once sufficient levels of chemokine diffuse to the source compartments, additional resting macrophages and T cells are recruited onto the lattice and migrate towards infected macrophages. Infected macrophages become chronically infected and then burst as their intracellular bacterial loads grow and eventually reach their carrying capacity. Bursting leads to spread of bacteria to neighboring compartments. Resting macrophages attracted to the site may be infected by extracellular bacteria leading to a repeat of the cycle just described and further spread of infection. On the other hand, if T cells have reached the neighborhood, newly infected macrophages may be activated, contributing to containment and even diminution of infection. The model dynamics are represented in the lung compartment portion of Figure 2.1 without dendritic cells. Full details are available in [62].

3.5.3. Results. By varying key parameters in the model influencing the dynamics summarized above we obtained a number of distinct outcomes of infection. The outcomes can be differentiated quantitatively according to total extracellular bacterial load on the lattice over the course of a simulation and, qualitatively, according to the spatio-temporal spread of infection. The outcomes can be classified as follows: bacterial *clearance*, bacterial *containment*, and bacterial *dissemination*.

For bacterial clearance to occur, both extracellular and intracellular bacteria are

completely eliminated, and there is almost no remanent of infection and inflammation on the lattice. (There may be a small number of necrotic sites due to isolated bursting and killing.) Clearance occurs when there is a strong effector T cell response, resulting in a large number of activated macrophages that are able to clear all bacteria.

For bacterial containment to occur (likely the most common outcome), the immune response succeeds in maintaining low levels of infected macrophages and avoiding the spread of infection to other sites. Extracellular bacteria persist but are spatially contained surrounded by macrophages and necrotic sites.

During dissemination, extracellular bacterial levels grow without bound, and infection spreads across the lattice due to bursting and killing. The system is unable to contain bacterial spread.

Figures 3.9 and 3.10 show results for total bacteria and macrophage levels on the lattice during two simulations representing two of the infection outcomes. Panels A show results from a simulation leading to containment, while panels B show the simulation leading to dissemination, after we decreased the value of T cell recruitment. In the containment simulation (Figure 3.9 A), extracellular bacteria (BE) are trapped by macrophages and necrotic sites, and BE is greater than intracellular bacteria (BI). Large numbers of extracellular bacteria are observed in the dissemination scenario (Figure 3.9 B). In containment, resting macrophages (MR) maintain a steady large value to keep the infection isolated (Figure 3.10 A). On the other hand, in dissemination the number of resting macrophages decrease after 100 days due to bursting or killing, and thus the system is unable to contain the spread of bacteria (Figure 3.10 B).
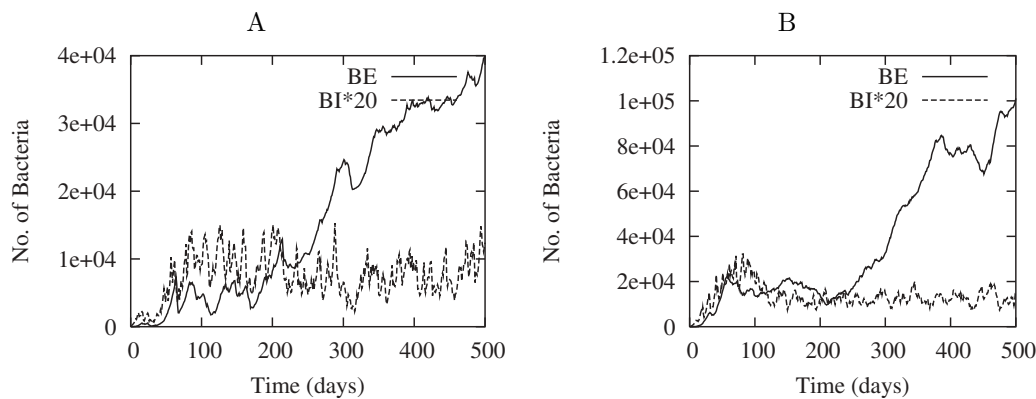

FIG. 3.9. Results of bacterial load from two simulations of the agent-based model. *Shown are both total extracellular bacteria (BE) and intracellular bacteria (BI); the latter has been scaled by a factor of* 20 *so that the results are on similar scales. Panel* A *shows containment of infection, while panel* B *shows dissemination.*

These temporal dynamics can be explained by examining the spatio-temporal progression of the simulations. Figure 3.11 shows snapshots of the lattice at various times during the same containment simulation used to generate panels A of Figures 3.9 and 3.10. As can be seen, infection initially spreads outwards in a roughly symmetrical pattern due to bursting of chronically infected macrophages. Resting macrophages (green) are activated (blue) by T cells (pink) to control infection. At 30 and 60 days a ring of infected macrophages (orange) is observed around extracellular bacteria (yellow). In the last snapshot, at time 360 days, extracellular bacteria are trapped
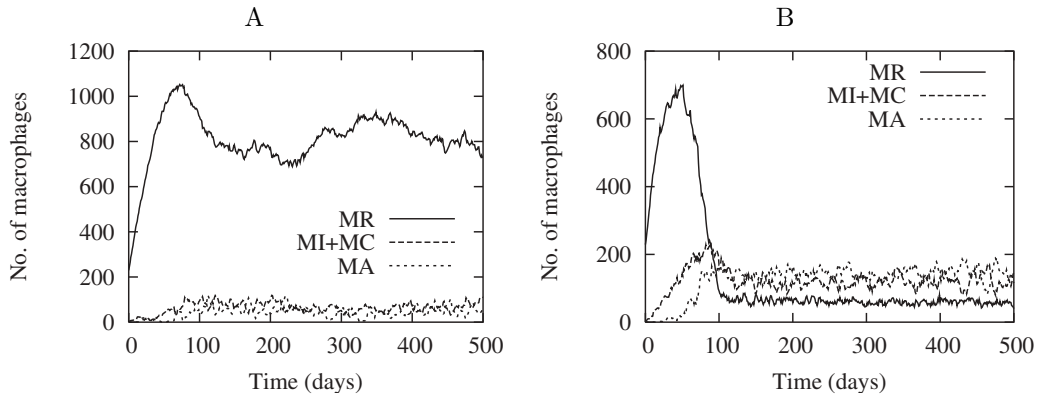
FIG. 3.10. *Results of macrophage populations from two simulations of the agent-based model.*
Shown are resting macrophages (MR), infected macrophages (MI), activated macrophages (MA),
and chronically infected macrophages (MC). Panel A *corresponds to containment of infection,*
while panel B *corresponds to dissemination.*

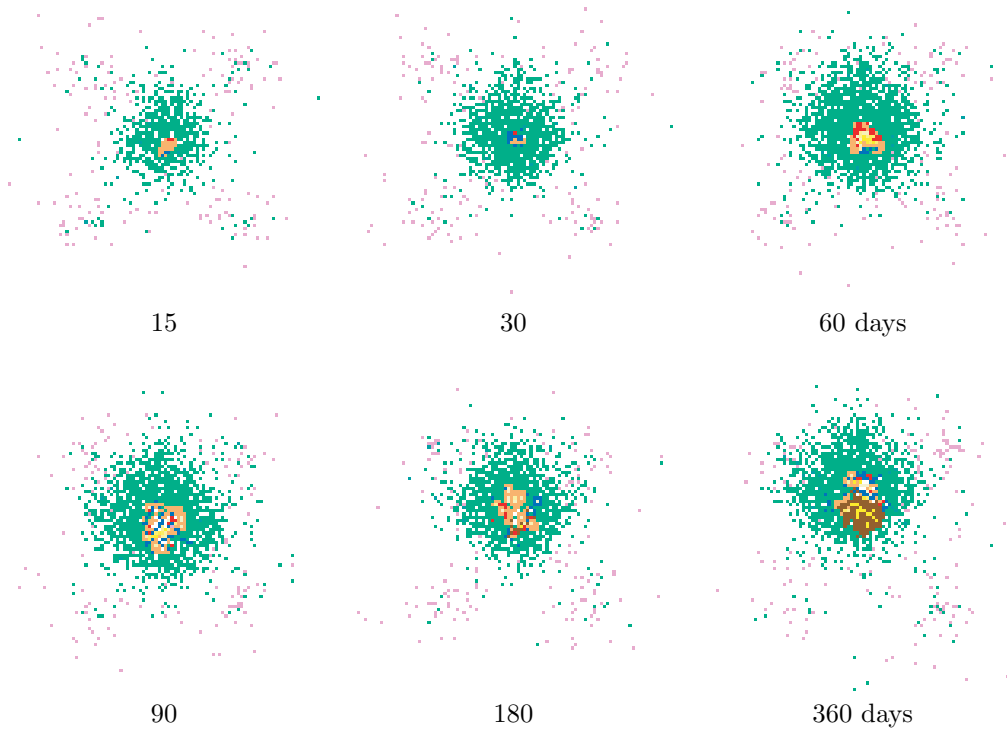FIG. 3.11. *Spatio-temporal snapshots of the lattice at times* $t = 15, 30, 60, 90, 180,$ *and* 360 *days*
during a simulation of the agent-based model leading to containment of infection. Colors correspond
as follows: bacteria (yellow), T cells (pink), infected macrophages (orange), chronically infected
macrophages (red), resting macrophages (green), activated macrophages (blue), and necrotic regions
(brown).

within a ring of macrophages and necrotic sites (in brown). A strength of the agent-based model is that it allows such visualization of the spatio-temporal dynamics of the model.

We identified numerous parameters in the model that can influence which infection outcome occurs. Our analysis shows that several parameters have positive or negative correlations with total extracellular bacteria levels. These results are summarized in Table 3.5. Interestingly, macrophage recruitment rates are *positively* correlated with extracellular bacteria levels. Higher levels of resting macrophages can lead to a detrimental outcome of infection for the host. This can be explained by a uniquely spatial phenomenon: a large number of resting macrophages crowded around infected macrophages hinders T cell proximity to infected macrophages. This limits activation of infected macrophages, causing them to become chronically infected, eventually bursting and leading to infection spread.

TABLE 3.5
Parameters which are positively or negatively correlated total extracellular bacteria (BE) based on PRC analysis. Parameters in the top half of the table are kinetic parameters, while the bottom half lists spatial recruitment and movement parameters at 500 days of infection. All correlations shown have a P-value < 0.001.

Parameter description	Correlation with extracellular bacterial load
Probability a T cell activates a macrophage	negative
Rate of macrophage recruitment	positive
Rate of T cell recruitment	negative
Probability of T cell movement next to a macrophage	negative
Rate of activated macrophage movement	positive

Indeed, the probability of T cell movement (into a macrophage occupied micro-compartment) and the rate of T cell recruitment both show a negative correlation with total extracellular bacteria, further demonstrating that T cell activity is essential for infection control. Our analysis of the PRC values for these two parameters shows that the probability of T cell movement is more significant than the rate of T cell recruitment (see [62]). This result is interesting, as it shows that the spatial distribution of T cells, and specifically their spatial proximity to infected macrophages, is more significant than their mere abundance. Note that it was the spatial scale of the agent-based model that led us to introduce a parameter related to T cell movement and allowed us to observe this crowding effect of macrophages with respect to T cells.

4. Comparison/contrast of results of different approaches. In each of the five sections, models were presented describing the immune response to Mtb. An outline of each model, together with key results, were highlighted. Here, we compare and contrast results obtained and explore what insights are gained using these different approaches. Table 4.1 presents a summary of model features for comparison. Elements such as mathematical formulation and design features are shown.

4.1. Baseline outcomes. Model results fall into two categories: global and local. Global results distinguish between latency and active disease. Local results distinguish between the development of a small, solid granuloma (containment of infection) and the development of a large necrotic granuloma (unchecked infection and spread). Figures in each of the sections present intracellular and extracellular bacteria loads and macrophage dynamics. We compare these results below. One interesting thing to note (as pointed out in the parameter analysis sections and discussions above) is that there exists multiple paths for the system to fail from latency

TABLE 4.1
Table summarizing features of the five models. Abbrev: C = continuous, D = discrete, S = stochastic, d = deterministic, LN = lymph node.

Model type	Dynam-ics	Environment	Global/local	Features
ODE	C,d	lung fluid (BAL)	global	Computationally easy, Math. complex, no spatial.
2-Compartment ODE	C,d	1 cm^3 lung and LN	global	Computationally easy, Math. complex, spatial.
Metapopulation	C,S,d	5mm x 5mm lung tissue	local	Computationally expensive, Math. less complex, spatial.
PDE	C,d	Lung tissue	local	Computationally expensive, Math. complex, less complex biologically, spatial.
Agent based model (ABM)	D,S	2mm x 2mm lung tissue	local	Computationally very expensive, Math. less complex, more biological features, spatial.

(or containment) leading to active disease (or disseminating infection). The dynamics presented in the figures are thus representative of each of the achievable infection outcomes; nonetheless, comparisons can be drawn between them as mathematical expressions and parameter values are preserved when possible.

4.1.1. Bacterial levels. In all the models we presented, extracellular bacteria load as a marker of infection progression (both local and global; compare panels A in Figures 3.1, 3.2, 3.4, 3.7, 3.9, and 3.10). In fact, these models provide a unique opportunity to track the location of bacteria (intracellular versus extracellular) that is not measured experimentally. In the first four models, during latency (or containment) intracellular bacterial load exceeds the extracellular load, while in disease (or disseminated infection) the bacterial load grows exponentially. In contrast, the agent-based model indicates that there is a larger number of extracellular bacteria than intracellular in both containment and disseminating infection (Figure 3.9). In both cases, the intracellular bacteria load remains in a quasi-steady state. This result follows in the agent-based model because the necrotic areas are facilitating the control of bacteria.

4.1.2. Macrophage levels. Regarding macrophage dynamics, clearly the levels of infected macrophages are indicators of infection status (at either local or global scales). Curiously, there are differences observed in macrophage levels between models. In the first model (see Figure 3.1, panels B), even high levels of activated macrophages are insufficient to suppress infection. In contrast, in the next two models (Figures 3.2 and 3.4, panels B) low levels of activated macrophages lead to infection. This implies that mechanisms other than macrophage activation are necessary for containment (or latency). This result is confirmed in experiment studies as well [17].

In all of the models, macrophage activation and their activity are essential for containment but are not sufficient. Even when the system is not able to contain bacterial growth, there are large amounts of activated macrophages present. This is also observed in the experimental and clinical setting [11, 20].

Upon examination of the tables for each of the models, we see further confirmation for a key role of macrophages in containment and latency outcomes (see Tables 3.1–3.5). In the two ODE models and metapopulation model, activation and infection rates are strongly correlated with outcome (correlation coefficients not shown). In the PDE model which represents the innate response, the ability of macrophages to take

up and kill bacteria plays a determinative role. Finally, in the agent-based model setting, although macrophage activation is still important, spatial dynamics become more relevant. This may explain why macrophage activation is necessary but not sufficient to contain infection [11, 20].

4.2. Parameters leading to distinct infection outcomes. In each model section, tables for relevant parameters are presented showing rates/rate constants that, if altered, lead to disease (disseminated infection) from latency (containment). There are both strong consistent themes and clear differences between the models. As the goal of this paper is to explore the spatial aspects of what controls immunity to TB, we focus on those parameters for our study.

Parameters that govern success or failure of the immune response in the first model depend largely on macrophage dynamics (Table 3.1). Interestingly, rates/ rate constants that indirectly represent recruitment of new cells to the site of infection are not key to determining outcome. Other processes that were represented in an indirect way did arise as important (such as the production of INF-γ from CD8$^+$ T cells, which we represented by a general source term). We have now developed an extended model to explore this topic more mechanistically [69].

In the two-compartment model, where we begin to more mechanistically explore some spatial aspects (more global ones than local ones, however), the trafficking of cells between the two compartments of blood and lymph, as well as recruitment rates of T cells, emerge as key (Table 3.2). Here we have replaced the indirect phenomenological representations of these processes from the first model with direct spatial representations.

Moving to the first more local spatialization model (the metapopulation model), recruitment of immune cells again emerges as key (global level recruitment). When adding local spatialization as well, the speeds at which cells and effector molecules affect movement on the lattice greatly influences infection dynamics (Table 3.3).

As discussed in section 3.4, the PDE model represents the innate response model to Mtb. Even in this state, recruitment of cells is key (Table 3.4). However, here chemokine levels needed to jumpstart the system in the right direction become relevant for the first time. Chemokines are included in the metapopulation model, but their rates do not arise as determinative in behavior outcome (Table 3.3).

The importance of both chemokines and cell movement are again observed in the agent-based model (Table 3.5). Interestingly, the ability of T cells to penetrate the granuloma structure to activate macrophages is key. This reveals a crowding effect of macrophage density on infection outcome. It is the spatial scale (local) at which the agent-based model is formulated that allows the study of this aspect of the organization of the immune response. This behavior emerges for the first time here since specific cell-cell interaction dynamics are best captured with this approach.

4.3. Model predictions. One of the key purposes of a mathematical model is to make predictions regarding the biological problem that is under study. Taken together, results from all five models suggest the following. First, a consistent theme from all five models was that of the role of macrophage activation and infection rates in infection dynamics. Activation is not surprising given that the importance of macrophage activation in TB infection is well established (see, e.g., [20]). What has not been discussed are infection dynamics. If infection could be slowed or halted, our results predict that containment or even clearance could occur. Studies with mutant bacterial strains of Mtb could confirm these predictions. Second, in the ODE models the ability of T cells to kill infected macrophages was of key importance. This implies

that once macrophages are infected, containment is completely under the control of T cells. Studies along these lines are already being performed by our experimental collaborators. This specific role for T cells became less pronounced in the spatial models, which we believe clouded these effects. Third, all of the spatial models identified a role for recruitment and movement of activated macrophages and also their ability to kill bacteria. Enhancing macrophage dynamics will certainly facilitate containment. Finally, chemokine dynamics are just being studied in the experimental setting. Our models predict that chemokine dynamics (turnover, diffusion rates, etc.) are all key to facilitating an optimal response. Factors that can enhance these features are likely to tilt the scale in favor of the host.

5. Discussion. One of the fundamental problems in using mathematics to model biological systems is choosing the appropriate scale representation. This work is an attempt to model a given biological system (namely the immune response to Mtb) using multiple scale approaches. To this end, we have applied a wide range of mathematical tools to explore a specific biological topic. In this way, we are able to compare and contrast the effects that scale has on the results. We applied continuous deterministic models (single and multiple compartment nonlinear ODE systems) to more discrete stochastic ones (an agent-based model) as well as approaches that fall in between (PDEs and metapopulation modeling). We presented baseline results in each scenario and contrasted the local and global spatial effects that were captured with each. Other groups have done similar comparisons (see, e.g., [41]), but our approach improves on others as it is comprehensive in both the mathematical and the biological scale.

Several mathematical challenges arose in the process of developing and analyzing these models. One of the key difficulties that emerged when modeling cell movement was that of infected macrophages. In two of the models (metapopulation and PDE) we made the assumption that infected macrophages remain stationary. This implies that the intracellular bacterial load within each also remains stationary, and thus we could track at any moment where these bacteria were located. If we allowed for infected macrophages to move, there was no easy way to simultaneously allow for movement of the intracellular bacteria load. This problem was easily solved in the agent-based model setting.

Additionally, higher-dimensional systems (two- or three-dimensional) are likely necessary to capture more biological realism. This adds significant complexity to the current models, and we plan to address this in future work as well. Additional problems are a lack of in vivo data for the entities involved, including physical parameters such as diffusion constants, decay rates, number and distribution of molecules and cells, etc. Further biological refinements can be easily incorporated into any of the models as data become available.

Finally, a general challenge for modelers is to build models that integrate features across scales. Processes occurring at the gene, cellular, and tissue levels operate in tandem, and thus developing models which capture these integrative process simultaneously across scales is a collective goal. We believe the work discussed here is a first step in this direction.

Our ultimate goal is to combine different modeling approaches to produce hybrid models that operate on different scales simultaneously. For example, if we introduced PDEs to describe the dynamics of the more continuous entities in the agent-based model (rather than the ODEs we presently model them with) we can allow for spatial actions of these variables as well. Another example would be to develop a multi-

ple compartmental agent-based model (i.e., combining the two-compartmental ODE model ideas with the agent-based model). Either of these approaches will likely give further insights into the biological mechanisms operating at different scales that yield a properly functioning granuloma.

6. Appendix.

6.1. Equations for the metapopulation model. In this appendix we present the equation for the metapopulation model discussed in section 3.3. As mentioned in section 3.3, local (within-compartment) interactions and the corresponding terms in the ODEs are adapted from [76], so the discussion of the equations below refers back to the equations presented in section 3.1. The movement terms for $M_{R\ (i,j)}(t)$, $M_{A\ (i,j)}(t)$, and $T_{(i,j)}(t)$ are initially denoted by $Mov_{(i,j)}^{w}(t)$ (for $w = M_R, M_A, T$) in the equations below. They are subsequently described in more detail.

6.1.1. Macrophage dynamics. The equations describing macrophage dynamics within each compartment (i, j) are given below (for readability we have suppressed the (t) notation in all equations):

(6.1)
$$
\begin{aligned}
\frac{d}{dt}M_{R\ (i,j)} \ &= (\delta_i + \delta_j)\left(S_{MR} + s_{chM}\left(\frac{C_{(i,j)}}{C_{(i,j)}+s_{chM0}}\right)\right) - k_2 M_{R\ (i,j)}\left(\frac{B_{E\ (i,j)}}{B_{E\ (i,j)}+c_9}\right) \\
&\quad - k_3 M_{R\ (i,j)}\left(\frac{T_{(i,j)}}{T_{(i,j)}+s_3}\right)\left(\frac{B_{T\ (i,j)}}{B_{T\ (i,j)}+c_8}\right) - \mu_R M_{R\ (i,j)} \\
&\quad + \mu_{da}M_{A\ (i,j)}\left(\frac{s_3}{T_{(i,j)}+s_3}\right)\left(\frac{c_8}{B_{T\ (i,j)}+c_8}\right) + Mov_{(i,j)}^{M_R},
\end{aligned}
$$

(6.2)
$$
\begin{aligned}
\frac{d}{dt}M_{I\ (i,j)} \ &= k_2 M_{R\ (i,j)}\left(\frac{B_{E\ (i,j)}}{B_{E\ (i,j)}+c_9}\right) - k_{17}M_{I\ (i,j)}\left(\frac{B_{I\ (i,j)}^2}{B_{I\ (i,j)}^2+\left(NM_{I\ (i,j)}\right)^2}\right) \\
&\quad - k_{14}M_{I\ (i,j)}\left(\frac{T_{(i,j)}/M_{I\ (i,j)}}{T_{(i,j)}/M_{I\ (i,j)}+c_4}\right)\left(1 - p\left(\frac{B_{I\ (i,j)}}{B_{I\ (i,j)}+NM_{I\ (i,j)}}\right)\right) \\
&\quad - \mu_I M_{I\ (i,j)},
\end{aligned}
$$

(6.3)
$$
\begin{aligned}
\frac{d}{dt}M_{A\ (i,j)} \ &= k_3 M_{R\ (i,j)}\left(\frac{T_{(i,j)}}{T_{(i,j)}+s_3}\right)\left(\frac{B_{T\ (i,j)}}{B_{T\ (i,j)}+c_8}\right) \\
&\quad - \mu_{da}M_{A\ (i,j)}\left(\frac{s_3}{T_{(i,j)}+s_3}\right)\left(\frac{c_8}{B_{T\ (i,j)}+c_8}\right) - \mu_A M_{A\ (i,j)} + Mov_{(i,j)}^{M_A}.
\end{aligned}
$$

In (6.1), δ_i and δ_j define the compartments in the spatial domain into which resting macrophage recruitment occurs. As resting macrophages are assumed to enter the site of infection only at the boundaries (see below), i.e., for $i = 0$ or $n-1$, $j = 0$ or $n-1$, δ_i and δ_j are defined as follows:

(6.4)
$$
\delta_i = \begin{cases} 1 & \text{if } i = 0 \text{ or } n-1, \\ 0 & \text{otherwise,} \end{cases} \qquad \delta_j = \begin{cases} 1 & \text{if } j = 0 \text{ or } n-1, \\ 0 & \text{otherwise.} \end{cases}
$$

The dynamics of each macrophage subpopulation ($M_{R\ (i,j)}(t)$, $M_{A\ (i,j)}(t)$, and $M_{I\ (i,j)}(t)$) are a simplified subset of the dynamics described in section 3.1. The major change is that the terms in the equations of that model are "relativized" to each compartment (i, j). This reflects that these dynamics now take place *locally* with respect to the spatial environment, i.e., within each compartment. Thus, resting macrophages $M_{R\ (i,j)}$ become infected in the presence of extracellular bacteria $B_{E\ (i,j)}$

in the same (i, j) *compartment* at a maximal rate of k_2. Similarly for activation of resting macrophages, deactivation of activated macrophages, bursting of chronically infected macrophages, and lysis of chronically infected macrophages by T cells. Note, however, that in the terms representing activation and deactivation, I_γ has been replaced by $T_{(i,j)}$. Cytokines such as IFN-γ were not included in this model, but their effects were represented by substituting the cell type that produces them, in this case T cells.

The most significant change in macrophage dynamics as compared to the temporal ODE model is in recruitment of new cells to the site of infection. In both models, macrophages are recruited to the site of infection via two separate mechanisms: (1) a constant source term that provides a baseline level of resting macrophages in the lung tissue, even in the absence of infection, and (2) recruitment of additional resting macrophages to the site of infection in response to chemokines released by infected and activated macrophages. Since the ODE models did not include chemokines, the latter type of recruitment was represented implicitly, via both the infected and activated macrophage variables. In that sense, chemokine recruitment was represented indirectly. Since chemokine variables were added to this model, we represented chemokine-driven recruitment explicitly. Thus, resting macrophages are recruited into a boundary compartment (i, j) in response to the value of $C_{(i,j)}(t)$ at a maximal rate s_{ch}; this is modified by a Michaelis–Menten function.

Finally, macrophage migration between adjacent compartments of the lattice is captured by a set of "movement terms," $Mov^w_{(i,j)}(t)$, $w = M_R, M_A$. These are included in the equations for both resting and activated macrophages ((6.1) and (6.3), respectively). A description of these movement terms is given below. We assumed that infected macrophages have a reduced ability to sense chemokine gradients and to move. Hence, infected macrophages do not move between compartments in this model.

6.1.2. T cell dynamics. The equation describing T cell dynamics within each compartment (i, j) is

$$
(6.5) \quad \begin{aligned}
\frac{d}{dt}T_{(i,j)} \quad &= (\delta_i + \delta_j)\ s_{chT}\left(\frac{C_{(i,j)}}{C_{(i,j)}+s_{chT0}}\right)\ +\ \alpha_2 T_{(i,j)}\left(\frac{M_{A\ (i,j)}}{M_{A\ (i,j)}+c_{15}}\right) \\
&\quad -\ \mu_T T_{(i,j)} +\ Mov^T_{(i,j)},
\end{aligned}
$$

where δ_i and δ_j are as in (6.4) and restrict T cell recruitment to the boundary compartments.

T cell dynamics are substantially simplified as compared to the temporal ODE model, since we collapsed the three T cell types of that to a single type. Additionally, we removed the dynamics of various cytokines present in that model. We include proliferation of T cells in the presence of activated macrophages, and we include natural death. Finally, as with resting macrophages as described above, we replace the indirect representation of chemokine-driven recruitment in the temporal ODE model by a direct representation using the new chemokine variables. As with resting macrophages above, such recruitment takes places only in the boundary compartment and is modified by a Michaelis–Menten function.

6.1.3. Bacterial dynamics. The equations describing bacterial dynamics within each compartment (i, j) are exactly as the bacterial dynamics equations for the temporal ODE model, relativized to compartment (i, j). We do not repeat them here.

6.1.4. Chemokine dynamics. The chemokine variables $C_{(i,j)}(t)$ represent an aggregate concentration of the various chemokines involved in granuloma formation. These chemokines are secreted by infected macrophages and activated macrophages at maximal rates of c_I and c_A, respectively. Chemokine decays at rate Γ_C. We modeled chemokine diffusion via two parameters: a rate of diffusion μ_c and a parameter α_C corresponding to the proportion of chemokine that leaves the compartment (i,j). This leads to the following equation for $C_{(i,j)}$:

$$
(6.6) \quad
\begin{aligned}
\frac{d}{dt}C_{(i,j)} \;&=\; c_I\left(\frac{M_{I\,(i,j)}}{M_{I\,(i,j)}+a_3}\right) \;+\; c_A\,M_{A\,(i,j)} \;-\; \Gamma_C C_{(i,j)} \;-\; \mu_c\,\alpha_C\,C_{(i,j)} \\
&\quad +\; \chi_c\left(\tfrac{\alpha_C}{4}\right)\left(\delta_R\,C_{(i-1,j)} + \delta_L\,C_{(i+1,j)} + \delta_D\,C_{(i,j-1)} + \delta_U\,C_{(i,j+1)}\right),
\end{aligned}
$$

where δ_R, δ_L, δ_D, and δ_U are defined as in (6.7) to indicate that there is no chemokine diffusion into the boundary compartments from outside the lattice.

$$
(6.7) \quad
\left.
\begin{array}{ll}
\delta_R = \begin{cases} 1, & i \neq 0, \\ 0 & \text{otherwise}, \end{cases} &
\delta_L = \begin{cases} 1, & i \neq n-1, \\ 0 & \text{otherwise}, \end{cases} \\[2.5ex]
\delta_D = \begin{cases} 1, & j \neq 0, \\ 0 & \text{otherwise}, \end{cases} &
\delta_U = \begin{cases} 1, & j \neq n-1, \\ 0 & \text{otherwise}. \end{cases}
\end{array}
\right\}.
$$

6.1.5. Movement terms. The movement terms $Mov^{w}_{(i,j)}$ that occur in (6.1), (6.3), and (6.5) (i.e., for $w = M_R$, M_A, or T, respectively) represent the chemotactic movement of these subpopulations from compartment (i,j) to the four neighboring compartments, i.e., up (U) to $(i,j-1)$, down (D) to $(i,j+1)$, left (L) to $(i-1,j)$, and right (R) to $(i+1,j)$ (see Figure 3.3), and vice versa. The movement terms take the following form:

$$
\begin{aligned}
Mov^{w}_{(i,j)}(t) \;=\; &-\overbrace{\chi_w\,(1-\alpha^{w}_{i,j,S})\,w_{(i,j)}}^{\text{movement out}} \;+\; \delta_R\,\overbrace{\chi_w\,\alpha^{w}_{i-1,j,R}\,w_{(i-1,j)}}^{\text{movement in from left}} \\
&+\; \delta_L\,\overbrace{\chi_w\,\alpha^{w}_{i+1,j,L}\,w_{(i+1,j)}}^{\text{movement in from right}} \;+\; \delta_D\,\overbrace{\chi_w\,\alpha^{w}_{i,j-1,D}\,w_{(i,j-1)}}^{\text{movement in from above}} \\
&+\; \delta_U\,\overbrace{\mu_w\,\alpha^{w}_{i,j+1,U}\,w_{(i,j+1)}}^{\text{movement in from below}} \; .
\end{aligned}
$$

The coefficients δ_l (for $l = R$, L, D, U), as defined in (6.7), are included so that only the appropriate movement terms appear in the equations for the boundary compartments. The parameter χ_w represents the rate of movement of cell type w. Finally, $\alpha^{w}_{i,j,S}$, $\alpha^{w}_{i,j,R}$, $\alpha^{w}_{i,j,L}$, $\alpha^{w}_{i,j,U}$, and $\alpha^{w}_{i,j,D}$ are a set of "movement coefficients" for cell type w in compartment (i,j). The algorithm by which the movement coefficients are calculated are discussed in detail in [22].

REFERENCES

[1] G. An, *Agent-based computer simulation and SIRS: Building a bridge between basic science and clinical trials*, Shock, 16 (2001), pp. 266–273.

[2] R. Axelrod, *The Complexity of Cooperation: Agent-Based Models of Competition and Cooperation*, Princeton University Press, Princeton, NJ, 1997.

[3] J. Banchereau, F. Briere, C. Caux, J. Davoust, S. Lebecque, Y. J. Liu, B. Pulendran, and K. Palucka, *Immunobiology of dendritic cells*, Annu. Rev. Immunol., 18 (2000), pp. 767–811.

[4] J. Banchereau and R. M. Steinman, *Dendritic cells and the control of immunity*, Nature, 392 (1998), pp. 245–252.

[5] S. M. Blower and H. Dowlatabadi, *Sensitivity and uncertainty analysis of complex models of disease transmission: An HIV model, as an example*, Internat. Statist. Rev., 62 (1994), pp. 229–243.

[6] G. Canetti, *The Tubercle Bacillus in the Pulmonary Lesion in Man*, Springer, New York, 1955.

[7] S. Capuano, D. Croix, S. Pawar, A. Zinovik, A. Myers, P. Lin, S. Bissel, C. Fuhrman, E. Klein, and J. Flynn, *Experimental Mycobacterium tuberculosis infection of cynomolgus macaques closely resembles the various manifestations of human M. tuberculosis infection*, Infection and Immunity, 71 (2003), pp. 5831–5844.

[8] S. Chang, J. Linderman, and D. Kirschner, *A role for multiple mechanisms in the inhibition of MHC class II-mediated antigen presentation by Mycobacterium tuberculosis*, Proc. Natl. Acad. Sci. USA, to appear.

[9] C. Chiu and F. Hoppensteadt, *Mathematical models and simulations of bacterial growth and chemotaxis in a diffusion gradient chamber*, J. Math. Biol., 42 (2001), pp. 120–144.

[10] G. W. Comstock, *Epidemiology of tuberculosis*, Am. Rev. Respir. Dis., 125 (1982), pp. 8–16.

[11] A. M. Cooper, D. K. Dalton, T. A. Stewart, J. P. Griffin, D. G. Russell, and I. M. Orme, *Disseminated tuberculosis in interferon gamma gene-disrupted mice*, J. Exp. Med., 178 (1993), pp. 2243–2247.

[12] L. DesJardin, T. Kaufman, B. Potts, B. Kutzbach, H. Yi, and L. Schlesinger, *Mycobacterium tuberculosis-infected human macrophages exhibit enhanced cellular adhesion with increased expression of LFA-1 and ICAM-1 and reduced expression and/or function of complement receptors, FcgammaRII and the mannose receptor*, Microbiol., 148 (2002), pp. 3161–3171.

[13] J. F. Emile, N. Patey, G. Altare, S. Lamhamedi, E. Jouanguy, F. Boman, J. Quillard, M. Lecomte-Houcke, O. Verola, J. F. Mousnier, F. Dijoud, S. Blanche, N. Fischer, A Brousse, and J. L. Casanova, *Correlation of granuloma structure with clinical outcome defines two types of idiopathic disseminated bcg infection*, J. Pathology, 181 (1997), pp. 25–30.

[14] J. Epstein and R. Axtell, *Growing Artificial Societies: Social Science from the Bottom Up*, Brookings Insititution Press, Washington, DC, 1996.

[15] G. Ermentrout and L. Edelstein-Keshet, *Cellular automata approaches to biological modeling*, J. Theoret. Biol., 160 (1993), pp. 97–133.

[16] I. Flesch and S. Kaufmann, *Activation of tuberculostatic macrophage functions by gamma interferon, interleukin-4, and tumor necrosis factor*, Infection and Immunity, 58 (1990), pp. 2675–2677.

[17] J. Flynn and J. Chan, *Immunology of tuberculosis*, Annu. Rev. Immunol., 19 (2001), pp. 93–129.

[18] J. L. Flynn, S. V. Capuano, D. Croix, S. Pawar, A. Myers, A. Zinovik, and E. Klein, *Non-human primates: A model for tuberculosis research*, Tuberculosis (Edinb.), 83 (2003), pp. 116–118.

[19] J. L. Flynn and J. Chan, *Tuberculosis: Latency and reactivation*, Infection and Immunity, 69 (2001), pp. 4195–4201.

[20] J. L. Flynn, J. Chan, K. J. Triebold, D. K. Dalton, T. A. Stewart, and B. R. Bloom, *An essential role for interferon-γ in resistance to Mycobacterium tuberculosis infection*, J. Exp. Med., 178 (1993), pp. 2249–2254.

[21] D. Gammack, C. Doering, and D. Kirschner, *Macrophage response to Mycobacterium tuberculosis infection*, J. Math. Biol., 48 (2004), pp. 218–242.

[22] S. Ganguli, D. Gammack, and D. Kirschner, *A metapopulation model of granuloma framework in the lung during infection with Mycobacterium tuberculosis*, Math. Biosci. Eng., submitted.

[23] E. Giacomini, E. Iona, L. Ferroni, M. Miettinen, L. Fattorini, G. Orefici, I. Julkunen, and E. M. Coccia, *Infection of human macrophages and dendritic cells with Mycobacterium tuberculosis induces a differential cytokine gene expression that modulates T cell response*, J. Immunol., 166 (2001), pp. 7033–7041.

[24] B. Grenfell, B. Bolker, and A. Kleczkowski, *Seasonality and extinction in chaotic metapopulations*, Proc. R. Soc. Lond., 259 (1995), pp. 97–103.

[25] V. Grimm, *Ten years of individual-based modelling in ecology: What have we learned, and what*

could we learn in the future?, Ecological Modelling, 115 (1999), pp. 129–148.

[26] P. Guermonprez, J. Valladeau, L. Zitvogel, C. Thery, and S. Amigorena, *Antigen presentation and T cell stimulation by dendritic cells*, Annu. Rev. Immunol., 20 (2002), pp. 621–667.

[27] J. Helton and F. J. Davis, *Sampling-based methods*, in Sensitivity Analysis, A. Saltelli, K. Chan, and E. M. Scott, eds., Wiley, Chichester, 2000, pp. 101–154.

[28] R. A. Henderson, S. C. Watkins, and J. L. Flynn, *Activation of human dendritic cells following infection with mycobacterium tuberculosis*, J. Immunol., 159 (1997), pp. 635–643.

[29] S. P. Hickman, J. Chan, and P. Salgame, *Mycobacterium tuberculosis induces differential cytokine production from dendritic cells and macrophages with divergent effects on naive T cell polarization*, J. Immunol., 168 (2002), pp. 4636–4642.

[30] T. Hofer, J. Sheratt, and P. Maini, *Cellular pattern formation during dictyostelium aggregation*, Phys. D, 85 (1995), pp. 425–444.

[31] P. G. Holt, *Antigen presentation in the lung*, Am. J. Respir. Crit. Care Med., 162 (2000), pp. 151–156.

[32] P. G. Holt and M. A. Schon-Hegrad, *Localization of T cells, macrophages and dendritic cells in rat respiratory tract tissue: Implications for immune function studies*, Immunology, 62 (1987), pp. 349–356.

[33] M. D. Iseman, *Tuberculosis therapy: Past, present and future*, Eur. Respir. J. Suppl., 36 (2002), pp. 87s–94s.

[34] C. A. Janeway and P. Travers, *Immunobiology: The Immune System in Health and Disease*, Current Biology/Garland, New York, 1997.

[35] A. Johansen, *A simple model of recurrent epidemics*, J. Theoret. Biol., 178 (1996), pp. 45–51.

[36] M. Keeling, *Modelling the persistence of measles*, Trends in Microbiology, 5 (1997), pp. 513–518.

[37] M. Keeling and C. Gilligan, *Bubonic plague: A metapopulation model of zoonosis*, Proc. R. Soc. Lond., 267 (2000), pp. 2219–2230.

[38] M. Keeling and C. Gilligan, *Metapopulation dynamics of bubonic plague*, Nature, 407 (2000), pp. 903–906.

[39] E. Keller and L. Segel, *Model for chemotaxis*, J. Theoret. Biol., 30 (1971), pp. 225–234.

[40] E. Keller and L. Segel, *Traveling bands of chemotactic bacteria: A theoretical analysis*, J. Theoret. Biol., 30 (1971), pp. 235–248.

[41] J. Koopman, S. Chick, C. Simon, C. Riolo, and G. Jacquez, *Stochastic effects on endemic infection levels of disseminating versus local contracts*, Math. Biosci., 180 (2002), pp. 49–71.

[42] A. Lanzavecchia and F. Sallusto, *Dynamics of T lymphocyte responses: Intermediates, effectors, and memory cells*, Science, 290 (2000), pp. 92–97.

[43] Y. Mansury and T. Deisboeck, *Emerging patterns in tumor systems: Simulating dynamics of multicellular clusters with an agent-based spatial agglomeration model*, J. Theoret. Biol., 219 (2002), pp. 343–370.

[44] Y. Mansury and T. Deisboeck, *The impact of "search precision" in an agent-based tumor model*, J. Theoret. Biol., 224 (2003), pp. 325–337.

[45] S. Marino and D. E. Kirschner, *The human immune response to Mycobacterium tuberculosis in lung and lymph node*, J. Theoret. Biol., 227 (2004), pp. 463–486.

[46] S. Marino, S. Pawar, C. L. Fuller, T. A. Reinhart, J. L. Flynn, and D. E. Kirschner, *Dendritic cell trafficking and antigen presentation in the human immune response to Mycobacterium tuberculosis*, J. Immunol., 173 (2004), pp. 494–506.

[47] K. A. McDonough, Y. Kress, and B. R. Bloom, *Pathogenesis of tuberculosis: Interaction of M. tuberculosis with macrophages*, Infection and Immunity, 61 (1993), pp. 2763–2773.

[48] M. D. McKay, W. J. Conover, and R. J. Beckman, *A comparison of three methods for selecting values of input variables in the analysis of output from a computer code*, Technometrics, 21 (1979), pp. 239–245.

[49] M. Myerscough, P. Maini, and K. Painter, *Pattern formation in a generalized chemotactic model*, Bull. Math. Biol., 60 (1998), pp. 1–26.

[50] Q. N. Myrvik, E. S. Leake, and M. J. Wright, *Disruption of phagosomal membranes of normal alveolar macrophages by the H37Rv strain of* Mycobacterium tuberculosis, Am. Rev. Respir. Dis., 129 (1984), pp. 322–328.

[51] NAG Ltd., *NAG Fortran Library Manual*, Mark 19 ed., The Numerical Algorithms Group, Downers Grove, IL, 1999.

[52] C. F. Nathan, H. W. Murray, M. E. Wiebe, and B. Y. Rubin, *Identification of interferon-γ as the lymphokine that activates human macrophage oxidative metabolism and antimicrobial activity*, J. Exp. Med., 158 (1983), pp. 670–689.

[53] M. Owen and J. Sherratt, *Pattern formation and spatiotemporal irregularity in a model for macrophage-tumour interactions*, J. Theoret. Biol., 189 (1997), pp. 63–80.

[54] M. OWEN AND J. SHERRATT, *Mathematical modelling of macrophage dynamics in tumours*, Math. Models Methods Appl. Sci., 9 (1999), pp. 513–539.

[55] K. PAINTER, P. MAINI, AND H. OTHMER, *Development and applications of a model for cellular response to multiple chemotactic cues*, J. Math. Biol., 41 (2000), pp. 285–314.

[56] E. RENSHAW, *The development of a spatial predator-prey process on interconnected sites*, J. Theoret. Biol., 94 (1982), pp. 355–365.

[57] C. RHODES AND R. ANDERSON, *Persistence and dynamics in lattice models of epidemic spread*, J. Theoret. Biol., 180 (1996), pp. 125–133.

[58] P. SANNOMIYA, R. CRAIG, D. CLEWELL, A. SUZUKI, M. FUJINO, G. TILL, AND W. MARASCO, *Characterization of a class of nonformylated* enterococcus faecalis-*derived neutrophil chemotactic peptides: The sex pheromones*, Proc. Natl. Acad. Sci. USA, 87 (1990), pp. 66–70.

[59] B. SAUNDERS AND A. COOPER, *Restraining mycobacteria: Role of granulomas in mycobacterial infections*, Immunology and Cell Biology, 78 (2000), pp. 334–341.

[60] T. SCHELLING, *Models of segregation*, American Economic Review, Papers and Proceedings, 59 (1969), pp. 488–493.

[61] T. SCHELLING, *Micromotives and Macrobehavior*, Norton, New York, 1978.

[62] J. SEGOVIA-JUAREZ, S. GANGULI, AND D. KIRSCHNER, *Identifying control mechanisms of granuloma growth during Mycobacterium tuberculosis infection using an agent based model*, J. Theoret. Biol., 231 (2004), pp. 357–376.

[63] K. SERTL, T. TAKEMURA, E. TSCHACHLER, V. J. FERRANS, M. A. KALINER, AND E. M. SHEVACH, *Dendritic cells with antigen-presenting capability reside in airway epithelium, lung parenchyma, and visceral pleura*, J. Exp. Med., 163 (1986), pp. 436–451.

[64] J. SHERRATT, *Chemotaxis and chemokinesis in eukaryotic cells: The Keller-Segel equations as an approximation to a detailed model*, Bull. Math. Biol., 56 (1994), pp. 129–146.

[65] J. SHERRATT, E. SAGE, AND J. MURRAY, *Chemical control of eukaryotic cell movement: A new model*, J. Theoret. Biol., 162 (1993), pp. 23–40.

[66] R. F. SILVER, A. LI, W. H. BOOM, AND J. J. ELLNER, *Lymphocyte-dependent inhibition of growth of virulent* Mycobacterium tuberculosis *H37Rv within human monocytes: Requirement for CD4+ T cells in purified protein-positive, but not in purified protein derivative-negative subjects*, J. Immunol., 160 (1998), pp. 2408–2417.

[67] R. F. SILVER, Q. LI, AND J. J. ELLNER, *Expression of virulence of* Mycobacterium tuberculosis *within human monocytes: Virulence correlates with intracellular growth and induction of tumor necrosis factor-α but not with evasion of lymphocyte-dependent monocyte effector functions*, Infection and Immunity, 66 (1998), pp. 1190–1199.

[68] R. D. STOUT AND K. BOTTOMLY, *Antigen-specific activation of effector macrophages by IFN-γ producing TH1 T cell clones*, J. Immunol., 142 (1989), pp. 760–765.

[69] D. SUD, J. FLYNN, AND D. KIRSCHNER, *The role of CD8+ T cells in the immune response to M. tuberculosis*, Archivum Immunologiae et Therapiae Experimentalis (AITE), submitted.

[70] R. VAN CREVEL, T. OTTENHOFF, AND J. VAN DER MEER, *Innate immunity to Mycobacterium tuberculosis*, Clin. Microbiol. Rev., 15 (2002), pp. 294–309.

[71] R. VAN FURTH, M. M. C. DIESSELHOFF-DEN DULK, AND H. MATTIE, *Quantitative study on the production and kinetics of mononuclear phagocytes during an acute inflammatory reaction*, J. Exp. Med., 138 (1973), pp. 1315–1330.

[72] J. M. VAN HAARST, H. J. DE WIT, H. A. DREXHAGE, AND H. C. HOOGSTEDEN, *Distribution and immunophenotype of mononuclear phagocytes and dendritic cells in the human lung*, Am. J. Respir. Cell Mol. Biol., 10 (1994), pp. 487–492.

[73] U. H. VON ANDRIAN AND C. R. MACKAY, *T-cell function and migration. Two sides of the same coin*, N. Engl. J. Med., 343 (2000), pp. 1020–1034.

[74] J. WARD AND J. KING, *Mathematical modelling of avascular-tumour growth*, IMA J. Math. Appl. Med. Biol., 14 (1997), pp. 39–69.

[75] J. WARD AND J. KING, *Mathematical modelling of avascular-tumour growth* II: *Modelling growth saturation*, IMA J. Math. Appl. Med. Biol., 16 (1999), pp. 171–211.

[76] J. WIGGINTON AND D. KIRSCHNER, *A model to predict cell-mediated immune regulatory mechanisms during human infection with Mycobacterium tuberculosis*, J. Immunol., 166 (2001), pp. 1951–1967.

[77] WORLD HEALTH ORGANIZATION, *WHO Report* 2001: *Global Tuberculosis Control*, Tech. report, World Health Organization, Geneva, Switzerland, 2001.

[78] M. ZHANG, J. GONG, Y. LIN, AND P. BARNES, *Growth of virulent and avirulent Mycobacterium tuberculosis strains in human macrophages*, Infection and Immunity, 66 (1998), pp. 794–799.